Late Pleistocene submarine mass movements: Occurrence and causes

Article *in* Quaternary Science Reviews · April 2007

DOI: 10.1016/j.quascirev.2006.12.011

CITATIONS
112

READS
288

3 authors:

Matthew J Owen
Global Maritime
29 PUBLICATIONS **772** CITATIONS
SEE PROFILE

Simon Day
University College London
82 PUBLICATIONS **3,685** CITATIONS
SEE PROFILE

Mark Andrew Maslin
University College London
351 PUBLICATIONS **24,704** CITATIONS
SEE PROFILE

ELSEVIER

Quaternary Science Reviews 26 (2007) 958–978

QSR

Late Pleistocene submarine mass movements: occurrence and causes

Matthew Owen[a,*], Simon Day[b], Mark Maslin[a]

[a]Environmental Change Research Centre, Department of Geography, University College London, Pearson Building, Gower Street, London, WC1E 6BT, UK
[b]Benfield UCL Hazard Research Centre, Department of Earth Sciences, University College London, Gower Street, London, WC1E 6BT, UK

Received 28 February 2006; accepted 19 December 2006

Abstract

An extensive study of Late Pleistocene continental slope submarine mass movements was undertaken. Twenty-six well-dated mass movements occurred during the last 45 ka BP in the North Atlantic sector. A latitudinal trend is observed: between 45 and 12 ka BP most events occur in the mid- to low-latitudes, post-12 ka BP high-latitude occurring events dominate. A cluster of events is associated with the Last Glacial sea level lowstand and Termination 1B. Further events are associated with Termination 1A and the Holocene. Prior to 23 ka BP no clear relationship with the ice core atmospheric methane record is observed, in contrast during and following the deglaciation there is a possible relationship with atmospheric methane. High-latitude mass movements are primarily controlled by cyrospheric-induced variations in sedimentation and local sea level. In high latitudes, the glaciation subdues mass movement activity through reduced seisimicity, sediment supply and ocean temperatures. Deglaciation increases the sediment supply, seisimicity and ocean temperatures, thus increasing the likelihood of continental slope failures. For example the Storegga event coincides with high isostatic uplift and postglacial seisimicity, while the Andøya and Trænadjupet events occur before and after the peak rates respectively. In contrast low latitudes experience greater risk of slope failures during glacial periods from falling sea levels, although during the deglacial and interglacial period there is a potential for failure from changes in deposition centres and rates, as well as warming ocean temperatures potentially leading to dissociation of gas hydrates. The ongoing rapid deglaciation of coastal Greenland and Antarctica and consequent rapid input of sediment, isostatic uplift, crustal stress release and warming bottom water temperature at the shelf break will increase the risk of continental slope failure in these regions.

1. Introduction

During the Late Pleistocene the continental margins have frequently experienced mass movement events; the largest of which have volumes in excess of 3000 km^3. These events constitute major natural hazards. A number of recent submarine landslides, such as Grand Banks (1929) and Sissano (1998) have generated locally destructive tsunamis (see Tappin et al., 2001) whilst prehistoric events such as the Storegga slide discussed below produced regionally destructive tsunamis comparable in scale to the 2004 Indian Ocean tsunami (see Lay et al., 2005). On an even wider scale it has been proposed that large continental slope mass movements can induce rapid climate change through the release of gas hydrate CH_4 (see Nisbet, 1990; Haq, 1998; Norris and Röhl, 1999; Kennett et al., 2003). Various possible causes have been suggested including: seismic events (see Laberg et al., 2000), gas hydrate destabilisation (Haq, 1998; Maslin et al., 1998, 2005), increased sedimentation and crustal warping (Maslin et al., 1998; Van Weering et al., 1998), and the role of shelfwide glaciations in influencing these other factors (Evans et al., 2005).

Links between mass movements and climate change have been considered. Haq (1998) argued that during sea level lowstands reduced hydrostatic pressure would cause gas hydrates in ocean sediments to destabilise causing mass movements and releasing CH_4 into the atmosphere; which would act as a negative feedback to global cooling. Increased temperatures would lead to deglaciation in high latitudes at which point CH_4 release would act as positive feedback to global warming (Nisbet, 1990; Haq, 1998; Kennett et al., 2003). It has also been proposed that climate change could drive mass movements through sea level change and isostatic adjustment leading to crustal warping

*Corresponding author.
E-mail address: m.owen@ucl.ac.uk (M. Owen).

0277-3791/$ - see front matter © 2007 Elsevier Ltd. All rights reserved.
doi:10.1016/j.quascirev.2006.12.011

or increased seismicity (Grantz et al., 1996; Maslin et al., 1998; Van Weering et al., 1998; Laberg et al., 2000).

This paper will investigate the relationships between mass movements and climate change. We focus in particular on the different relationships between the two that may exist in particular regions (for example at high latitudes as compared to low latitudes) or at different stages in the glacial to interglacial climate cycle. These spatial and temporal variations in continental slope mass movement occurrence are, we argue, the key to understanding the underlying mechanisms of climate–mass movement interaction both through variations in the mechanisms that trigger mass movements and through variations in the susceptibility of slopes to failure under different climate conditions.

2. Controls on slope failure: susceptibility to failure and triggering of failure

Sediments fail when downslope (shear stress) force exceeds the resisting (shear strength) force. Sediments deposited in a state where shear strength exceeds shear stress will be stable. However, an alteration of this state, through either a reduction in sediment shear strength or through an increase in shear stress operating on that sediment, can lead to failure (see Biscontin et al., 2004). From a geological perspective, we distinguish two distinct categories of process that combine to produce the change in state from stable slope to failure and mass movement.

For a slope to fail, it must first be susceptible to failure. This is a product of geological history and local environmental conditions. For example the development of a low porosity layer, in an otherwise relatively porous environment, will lead to an increase in susceptibility to fail through prevention of pore water expulsion (during sedimentary loading) and the development of overpressure (see Dugan and Flemings, 2000; Volpi et al., 2003; Biscontin et al., 2004). Sedimentation patterns, glacial history and geological uplift are all factors that may influence a slope's susceptibility to fail without actually triggering a mass movement, or failure, event.

There is a distinction between factors increasing susceptibility to failure and those, which trigger the event. Actual failure occurs when a susceptible slope is affected by a triggering mechanism sufficient to destabilise it. Trigger mechanisms tend to be identifiable events with clear temporal constraints. For instance an earthquake, or destabilisation of a gas hydrate reservoir. This trigger will then influence the slope's geometry or sedimentological properties causing it to fail. During an earthquake seismic shaking leads to vertical and horizontal movement which increases the gravimetric forces operating on the sediments and the pore pressure: reducing the sediment shear strength allowing failure to occur (see Wright and Rathje, 2003; Martel, 2004; Strout and Tjelta, 2005).

Climate change and mass movement may, therefore, interact in the first instance through the effect of climate upon susceptibility to failure of sedimented slopes, or through the effect of climate upon the occurrence and intensity of triggering events. The effect upon climate of the slope failures then has the potential to act either as a positive or as a negative feedback upon the primary (climate driven) interaction.

2.1. Susceptibility factors

Susceptibility factors are those, which influence the long-term likelihood of a slope to fail.

In high latitudes, the advance and retreat of large ice-sheets influences the adjacent continental slopes' susceptibility to failure through a variety of mechanisms.

A slope's failure susceptibility is increased by isostatic uplift. The uplift of the continental side of the slope, coupled with the flooding of the ocean basins (by rising sea level) leading to basin subsidence, causes slope steepening (see Van Weering et al., 1998). A steeper slope increases the downslope gravimetric forces (the shear stress) increasing the likelihood of failure. Submarine landslides can originate on nearly flat surfaces. Slope angles on the Mississippi delta are generally $<0.4^{\circ}$, in this area mudslides caused by Hurricane Camille (1969) destroyed two platforms (see Bea et al., 1983) and mudslides have been documented on angles of 0.01° (see Hampton et al., 1996 and references cited within; Coleman et al., 1998; Walsh et al., 2006). A change in slope angle of $<1^{\circ}$ can be very significant in terms of a slope's engineering safety factor and its susceptibility to fail.

Rapid sedimentation and variation in sedimentation type as associated with the glacial cycles leaves a distinct sedimentary column. During interglacials pelagic sedimentation tends to dominate. This produces clays, silts and muds: sediments associated with high water content. During glacials and particularly during deglaciation, glaciogenic sedimentation dominates. This is associated with a very rapid input of terrigenous sediments (see Dowdeswell and Elverhøi, 2002). Deposited on top of soft pelagic muds, the glaciogenic sediment will compact them and force the pore fluids out of the pore spaces and into migration. However, upon reaching the less permeable glaciogenic sediment, overpressure will build up causing a reduction in sediment shear strength and the development of a weak layer (see Orange and Breen, 1992; Dugan and Flemings, 2000; Volpi et al., 2003; Strout and Tjelta, 2005). A contrast must be drawn, on glaciated margins, between sedimentary fan locations and inter-fan locations. Work on the svalbard margin by Dowdeswell and Elverhøi (2002) demonstrates that the fan areas are characterised by major sedimentary input during full glacial conditions. Inter-fan areas, however, receive high rates of sedimentation with the glacial advance, very low sedimentation during the LGM and then a rapid increase in sedimentation rates during the deglaciation. Return to interglacial conditions during the Holocene is associated with low rates of sedimentation.

It is also important to consider sequences of units. Multiple glacial–interglacial cycles build up alternating undercompacted units and low-permeability barriers. Periglacial outwash deposits (silts and sands) tend to have high permeability and porosity, the rapid rates of deposition lead to inefficient compaction. The muds and hemipelagic sediments, which follow, will tend to have a lower permeability due to lower rates of deposition and more efficient compaction. Owing to the lofting of buoyant meltwater (once coarser sediment has been deposited) there is the potential for developing thick, highly permeable and porous units immediately below interglacial muds (see Hesse et al., 2004). Sediments deposited may lack fine-grained fraction. Once these units are loaded and overpressured by sediment deposition in the next glacial cycle there is a potential for failure.

On the Norwegian margin contouritic sediments are important in determining the susceptibility of the slope to future failure. Infill drift contourites are deposited in existing slide scars (Bryn et al., 2005). They smooth the rough seabed created by the mass wasting processes and produce thick sediment bodies with high water content, which generate excess pore pressure when rapidly loaded by glaciogenic sediment. Bryn et al. (2005) conclude that the distribution of contourite drifts will influence the position of the next generation of slides.

In order to understand a slope's susceptibility to failure it is important to consider the slope and its sediments at the granular level. According to Orange and Breen (1992) the forces acting at this scale are: gravity, seepage force (drag asserted by fluid flow through a porous medium) and the frictional and cohesive strength of the material. Locat et al. (2004) use the Mohr–Coulomb failure criterion to calculate slope failure:

$$\tau = c' + (\sigma - u)\tan\,\phi',$$

where τ is the shear strength mobilised along the failure plane; c' is the cohesion; σ is the total stress; u is the pore pressure; and ϕ' is the friction angle. The stability of the slope is determined by the balance of the destabilising forces (downslope component of gravity, seepage forces, pore fluid pressure) and the stabilising forces (slope—normal component of gravity × friction coefficient, cohesion). The balance between these is in engineering terms the factor of safety (F, the ratio of the two sets of opposing forces). As F decreases the susceptibility to failure increases as the additional, transient seismic or fluid pressure force needed to produce failure decreases (also see Sultan et al. (2004) for discussion of factor of safety).

Sedimentation and alteration to the biogeochemcial properties of the sediments can increase the values of seepage force (and fluid migration), frictional strength of the material (cohesion), pore pressure and the total stresses can be changed via sedimentological processes.

Pore pressure is the pressure of the fluid within the pore spaces between soil grains (Strout and Tjelta, 2005). Increased pore pressure reduces the capacity of sediments to resist shear stresses and increases the likelihood of failure (see Biscontin et al., 2004; Strout and Tjelta, 2005). Several environmental changes may lead to overpressurisation through rapid sedimentation: pelagic, contouritic and glaciogenic (see Dugan and Flemings, 2000; Bryn et al., 2005; Strout and Tjelta, 2005). A slope may be made susceptible to failure, due to excess pore pressure, because of its sedimentation history.

Under the conditions associated with a homogeneous sedimentary column, deposited at a constant rate with constant porosity the sediments will compact, due to increased gravity loading, and the pore fluids will migrate up the column. The presence of faults and less permeable layers will, however, alter the migration. Faults channel the flow (see Volpi et al., 2003). Less permeable layers initially prevent vertical passage, and create overpressure beneath the cap, and then potentially also channel the flow beneath the cap creating a lateral flow until a weakness in the overlying layer is found, when vertical migration can recommence (see Fig. 1; and Orange and Breen, 1992; Dugan and Flemings, 2000; Volpi et al., 2003).

Diagenetic modification of sediments may also increase susceptibility to failure. Work by Volpi et al. (2003) investigating biogenic silica compaction demonstrates this. The transformation of Opal-A to Opal-CT is associated with a porosity reduction of ~20%, consequently an overpressurised layer occurs beneath this diagenetic front. Seismic profiles provide evidence of fluid vents rising from this boundary, in addition to evidence of surface layer creep (see Volpi et al., 2003).

Bacteria generate methane (biogenic) from the breakdown of organic-rich sediments deep in the sedimentary column, this can migrate upwards to form clathrates, forming methane hydrate (see Mienert et al., 1998; Dickens, 2003). Thermogenic methane may also migrate upwards in the sedimentary column. The clathrates strengthen the sediments but the free gas (a reservoir of which may form beneath the hydrate layer) will significantly weaken the sediments increasing the likelihood of failure (see Haq, 1998; Mienert et al., 1998; Sultan et al., 2004). Gas hydrates may only occur in high-pressure and low-temperature regimes, an increase in temperature or a reduction in pressure can cause the hydrate bonds to destabilise, releasing the caged-gas molecules (see Mienert et al., 1998; Dickens, 2003) and reducing the strength of the sediment. Hence the development of gas hydrates will increase the susceptibility of a slope to fail especially after long periods of free gas accumulation beneath the hydrate layer and when environmental conditions change to destabilise the hydrate layer.

As well as the micro-scale (granular) it is also necessary to consider the meso- and macro-scales. During and since the Miocene parts of the northwest Eurasian Plate have been subject to significant uplift (Stoker et al., 1994). This, as well as, the increased erosion associated with the Plio–Pleistocene glacial cycles led to the development of many fan complexes including the Barra, Donegal and

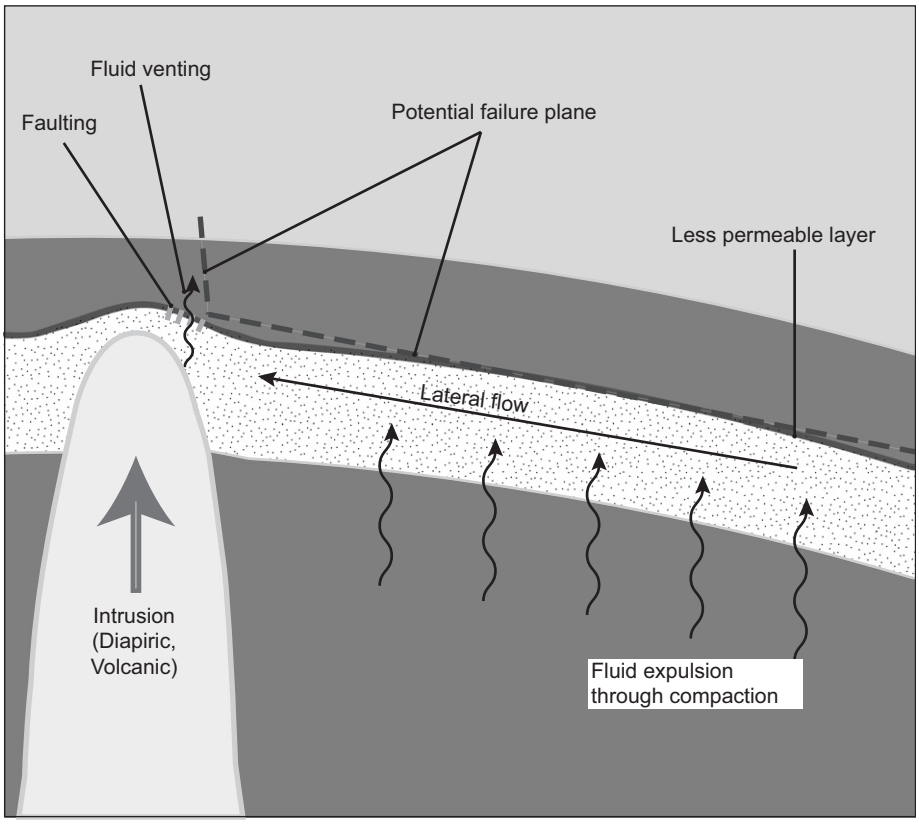

Fig. 1. Development of a failure plane through overpressure, permeability variation and fluid flow.

North Sea Fans (see Wilson et al., 2004; Bryn et al., 2005). It can be argued that the most important factor in a slope's susceptibility to failure is a supply of sediment to fail. As such in the case of the Barra, Donegal and North Sea Fans continental uplift and the onset of Pleistocene glacial cycles (with the associated increase in sedimentation) could be said to be the primary influence of susceptibility. Volcanic uplift would exert a similar, more localised, effect.

From whichever source it is derived, uplift will increase the slope angle and the gravimetric forces acting on a slope: further increasing failure susceptibility.

In low latitudes continental slope susceptibility to failure is primarily governed by sediment supply: through changes in deposition rates and centres. Sedimentation rate, on the continental shelf and slope in low latitudes, is influenced strongly by onshore climate and marine productivity. For example in the South China Sea glacial stages are marked by an increase in the aridity over northern Asia and a strong aeolian sediment input; while interglacials are associated with a stronger summer monsoon (with enhanced precipitation) resulting in greater physical erosion and chemical weathering (Boulay et al., 2005). Marine productivity influences the rates of pelagic sedimentation, and in the tropics is primarily governed by nutrient availability. This can be increased through intensified upwelling (see Little et al., 1997), as observed during the LGM on the Benguela margin and increased supply of terrigenous sediment (see von Rad and Tahir, 1997), as observed on the Indus shelf during the early Holocene.

Changes in sediment deposition centres will also effect low latitude continental slope susceptibility to failure through both changing slope angle and influencing pore pressure, and pore fluid migration. During lowstands river fan systems tend to bypass deltas and deposit fluvial, silty, clays directly onto the upper slope (see Amazon fan (Maslin et al., 1998), Indus fan (von Rad and Tahir, 1997), Bengal fan (Weber et al., 2003) and Pearl River fan (Boulay et al., 2005)). Potentially acting as a less permeable layer and a barrier to pore fluid migration. The fans are also subject to erosion, or aggradation, at different times. The Indus fan, for instance, was subject to massive erosion during the LGM, when there was extensive turbidite and slumping activity, during the Younger Dryas it aggraded and since the Holocene there has been relatively little activity (Von Rad and Tahir, 1997).

2.2. Triggers of slope failure

An action that initiates failure is termed a trigger.

Expansion and contraction of the cyrosphere affects seisimicity in high latitudes. The removal of the ice-mass releases stresses accumulated through long-term tectonic deformation: glaciation tends to be associated with aseismicity and the deglaciation with a pulse of seismic activity (Bungum et al., 2005 and references cited therein).

In the deglacial and postglacial environment, the largest earthquakes are likely to be found around the margins of the rebound dome, in the case of fennoscandia: in the northwest quadrant of the former forebulge (Muir-Wood, 2000). Work by Fjeldskaar et al. (2000) reinforces this. They predict the transition zone between uplift and subsidence to be located just offshore western Norway, as they note, the location where bending stress of the crust will be greatest.

Seismic triggers are defined as any motion of the earth (see Wright and Rathje, 2003; Biscontin et al., 2004). Acceleration-induced sliding occurs when strong seismic motions subject the sediments to horizontal and vertical accelerations, however, liquefaction-induced sliding occurs when cyclic shearing weakens the sediments (Wright and Rathje, 2003). Seismic shaking will generate excess pore pressure and it is possible for upward migrating pore fluid to cause an instability beneath a region with a lower dissipation rate (Biscontin et al., 2004). Slope failure may occur several months after the seismic event because the time required to reach critical conditions from different soil profiles range from minutes to months according to the corresponding coefficient of the consolidation profile, which will influence the dissipation rate (see Wright and Rathje, 2003; Biscontin et al., 2004).

Storm wave, or tsunami, loading may also trigger failures (see Jeng, 2001). Water waves generate adjacent zones of high- and low-pressure beneath crests and troughs, shear stress is generated between these zones (Hampton et al., 1996). Tsunami wave fronts are capable of generating large hydrodynamic pressures on the seafloor with the potential to lead to failure (see Wright and Rathje, 2003). An example is demonstrated by the work of Bea et al. (1983) in the Gulf of Mexico. Storm waves produced during the passage of Hurricane Camille (August 1969) triggered sediment failure to a depth of 30 m, lateral movement exceeded 1000 m (see Bea et al., 1983). Other examples of wave-induced sediment failure are discussed by Jeng (2001). Storm occurrence is also controlled temporally by climate, in high latitudes by the movement of the polar front and in low latitudes by the development of high-altitude zonal winds that tend to shear off hurricane systems.

Rapid drawdown of water, for instance by the approach of a tsunami, removes the resisting forces exerted by the water and induces undrained loading conditions, potentially causing failure (see Wright and Rathje, 2003). The Skagway slide and Fjord tsunami in Alaska (1994) seems to have been initiated by an exceptionally low tide (see Rabinovich et al., 1999).

Gas hydrate destabilisation can trigger slope failure. Distribution and stability of hydrates are controlled by: temperature, pore pressure, gas composition and pore water salinity (Kvenvolden, 1993, 1998). Any change in these parameters may lead to the conversion of hydrate into free gas plus water (see Sultan et al., 2004). This conversion reduces cohesive strength by removing hydrate cement and raising pore pressure. There are two ways that changes in the oceans may lead to gas hydrate destabilisation. Firstly, a reduction in pressure through a drop in sea level: it has frequently been argued that the sea level lowstand, associated with glacial conditions, could result in gas hydrate destabilisation, with the associated free gas release (see Nisbet, 1990; Haq, 1998; Kennett et al., 2003). Secondly, through an increase in ocean temperatures (as associated with the deglaciation or warm interstadials) causing destabilisation of the hydrate sediments (see Kennett et al., 2003; Mienert et al., 2005). In either case methane gas is released from the oxygen–hydrogen bonds creating a weak layer in the sedimentary column.

Failure may also be triggered by sediment deposition and the associated increase in pore pressure. For instance: vertical fluid migration is initiated by sediment consolidation, a less permeable layer is encountered leading to high pore pressure, eventually this fluid maybe expelled by venting (see Volpi et al., 2003). This loading process has produced a failure plane of reduced shear strength. As the downslope force gradually increases failure could be triggered, by the very gravimetric loading that has created the failure surface, at the moment when the driving downslope force exceeds the resisting shear strength (see Hampton et al., 1996).

Differences in patterns of triggering events can be seen between the high and low latitudes. There is a relative absence of postglacial seismicity in lower latitudes compared to abundance in higher latitudes. In lower latitudes hurricane frequency and alterations in sedimentation patterns are more significant trigger control mechanisms.

Cyclic variation in frequency and/or severity of triggering events may in itself produce particularly large failure events. A low-triggering period allows time for build up of susceptible sediment sequences that are then subjected to a period of high triggering event activity. This may explain the comparative absence of large-scale mass movement events on highly active margins, and locations (such as the Makran Margin of southwest Pakistan (see Prins and Postma, 2000), and the greater frequency of such events in less active locations (such as the Sindh margin, the Northwest European margin and the Amazon fan).

2.3. Results of slope failure

In addition to the creation of slump and slide scars on continental margins, and turbidite sands on the abyssal plains, slope failures have two major consequences: gas hydrate release and tsunami generation.

2.3.1. Gas hydrate release

A consequence of a mass movement occurring within, or adjacent to, clathrate bearing sediments is the possible release of gas hydrates. Release of this gas (commonly CH_4 or CO_2) into the atmosphere could have significant impact on global climate, for example the K/T event (Day and Maslin, 2005), the PETM (Norris and Röhl, 1999; Zachos

et al., 2001) and abrupt termination of the Pleistocene glaciations (Paull et al., 1991).

The specific mechanisms of failure triggering are also important in localising the failure plane above, within or below the zone of gas hydrate stability. They may also determine whether the developing failure becomes disintegrative, producing a disaggregated mass of sediment, or whether much of the sediment remains as slabs of coherent sediment. Gas hydrate embedded within the latter is carried down into deeper water and thus in general further into the stability field of solid gas hydrate.

The principal mechanism of hydrocarbon release from such failures is therefore not from the cohesive sediment masses themselves, but from uncapped reservoirs of free gas in the sediments below the failure plane and to a lesser extent from decompressed gas hydrates also originally located below the failure plane (known as the champagne cork effect).

In contrast, disintegrative slope failures (Hampton et al., 1996) typically develop into large-volume turbidity currents or grain flows. In such cases, while dense lithic grains settle out as ocean floor deposits, low-density, buoyant hydrate clasts will tend to rise in the water column and ultimately float upwards through the low-pressure limit of hydrate stability and there decompose releasing methane to the surface layers of the ocean or even directly to the atmosphere. On a small-scale, such floating may involve individual gas hydrate grains or nodules as demonstrated experimentally by Paull et al. (2003). On a larger scale in turbidity currents, buoyant gas hydrate grains would tend to rise in the turbidity currents and perhaps even produce convective lift-off of the turbidity current once a sufficiently high fraction of the sediment grains had settled out, in the reverse process to the rapid sinking of dense sediment laden plumes (Carey, 1997).

Large-scale lift-off of buoyant plumes from turbidity currents, equivalent to the buoyant rise of hot ash clouds from pyroclastic flows (Sparks et al., 1993), have been inferred from the characteristics of graded hemipelagic mud layers associated with the giant freshwater turbidites produced by meltwater discharge 'Heinrich' events from the Laurentian ice-sheet (Hesse et al., 2004). Association of such layers with disintegrative continental slope sediment failures (as far as the authors are aware, these layers have not yet been observed in conjunction with continental slope failure deposits) would provide direct evidence of escape of buoyant plumes from such failures and, therefore, plausible evidence for gas hydrate release.

2.3.2. *Tsunami generation*

Tsunamis are one of the more visible impacts from submarine mass movement: during the twentieth century tsunamis generated by mass movements on the continental slope have been linked to 27 deaths in Newfoundland (see Locat, 2001) and 2000 deaths in Papua New Guinea (see Tappin et al., 2001).

The magnitude of a tsunami generated by a submarine mass movement is dependent on the initial volume of the mass movement, seafloor geometry, the cohesion of the displaced mass, acceleration and velocity of the mass movement (Locat et al., 2004). The sediment type is also an important consideration: stiff clays will convert more of the mass movement's energy into tsunami energy, and are thus more likely to produce a tsunami than less dense, less compacted and more heterogeneous sediments (Tappin et al., 2001).

As with gas hydrate release, whether or not the mass movement is disintegrative or cohesive is a very important factor in tsunami generation. The more disintegrative the mass movement the less efficient it will be at displacing water and generating a wave front (see Tappin et al., 2001; Garagesh et al., 2003; Locat et al., 2004). However, a cohesive slide mass may not travel as fast as a disintegrative one. There is a tradeoff between cohesion of the sliding block and its basal friction, hence the velocity that it can attain. The true impact of the tsunami will not simply be a function of its size, but also of the region where it impacts. A large tsunami impacting on an uninhabited coastline will have a less severe impact than a smaller tsunami impacting on a densely inhabited coastline. As previously mentioned, tsunamis may have the additional effect of triggering submarine slope failures, and potentially generating more tsunamis.

3. Database

This study is based on an extensive review of scientific evidence for the timing and causes of submarine mass movements. The first stage was the development of a database of well dated North Atlantic sector large-scale submarine mass movements for the last 45 ka, first presented by Maslin et al. (2004).

The relationships between mass movements and CH_4, glacial cycles, and local and global sea level are discussed. Several fields are incorporated in the mass movement database and Table 1 summarises these and the reason for their inclusion.

The dataset produced using these methods consists, at its most basic, of timing and volume/mass of mass movements during the past 45 ka. Exact age determination is vital; an error of a thousand years may make the difference between rising and falling sea level, or a CH_4 peak or trough. We have developed a reliability index to examine the possible effect of these errors. The reliability index (see Table 1) is not attempting to grade any research; rather it reflects the difficulty of dating a particular mass movement emplacement. For example dating a megaturbidite, in a basin plain where sedimentation rates are known is a great deal more straightforward to date than a debris flow in a river fan that has been subjected to erosion during periods in its history. The reliability index is a five-point scale as follows: (1) excellent reliability, (2) good reliability, (3) average reliability, (4) mediocre reliability and (5) poor reliability.

Table 1
Explanation of mass movement database fields

Field	Reason for inclusion
Ocean/sea location	In order to allow an appreciation of geographical patterns and to locate the event
Specific location	As above
Latitude	As above, but also to allow a glacial component to be considered
Event name	To simplify discussion and general comprehension
Mass movement type	Being a mass movement database it contain many varieties of deposits (landslides, turbidites, and so on) and it is important to understand these differences and realise that different triggers may cause different types of failure
Radiocarbon age	The majority of timing estimations for this period (0–45 ka) have used ^{14}C dating
Calendar age	Dates may be in ^{14}C years but ice core and sea-level data are expressed in calendar years. Conversion was performed using Calib4.3 (Stuiver and Reimer, 1993)
Dating method	Despite the dominance of ^{14}C dating other techniques, with different reliabilities and assumptions, are used and it is important to be aware of these
Reliability index	Reflecting the difficulty in dating mass movements accurately. Some are easier to date than others, the more reliable the date, the more analytical weight which can be placed upon it (see text)
Volume	Simply demonstrating the different magnitudes of events
Mass	As above, but this field also allows a consideration of quantity of carbon release
Reference	Major reference providing information regarding event location, dimensions (with volume) and timing
Author(s) ascribed cause	Adding to potential cause and effect analysis as well as providing some insight into the initial author(s) findings
Notes	Cataloguing the work undertaken in database construction, such as assumptions, extrapolations and any other information used (including reference)

Some published dates have simply not been used due to doubt over their validity and more recent work, for example the omission of the Embley (1982) date for the Saharan sediment slide because of more recent research published by Gee et al. (1999).

Many problems are encountered when dating submarine mass movements, as demonstrated in Fig. 2. The most reliable method for determining emplacement dates, during the last 45 ka, is AMS ^{14}C dating pelagic sediment immediately above the deposit, as this should have been deposited immediately after emplacement. Material below the deposit will include reworked older material and the deposit itself will consist of sediment deposited prior to failure. It is not always possible to obtain dates from immediately above the deposit. In some instances timings are ascertained through extrapolations from sedimentation rates; but it should be noted that these are not always continuous. Moreover, the hemipelagic sedimentation above the slide maybe so rapid as to not contain enough dateable "pelagic" material. Alternatively, where a mass movement from shallow water is emplaced in much deeper water it may be preferable to pick abyssal-depth dwelling benthic foraminifera to date, in order to eliminate contamination of the dated samples from slide material (which should not contain the abyssal dwelling species).

The effect of bioturbation on AMS ^{14}C dates can lead to substantial error. Benthic organisms are known to burrow up to 10 cm into the ocean sediments (Loubere et al., 1995), this means that sediments of different ages can be mixed and in areas of low sedimentation rates, dating accuracy greatly reduced. Where a mass transport deposit has a low carbonate content there will be unequal bioturbation, as little carbonate is available to be mixed upwards and this younger material will be preferentially moved downwards, so AMS ^{14}C dating will under-represent the age of the event. Where the mass transport deposit has high carbonate content there may be equal bioturbation, but older carbonate will be bioturbated upwards making the age of the slump too old (see Fig. 2c). Published AMS ^{14}C dates, although acquired through sound research, may be inherently inaccurate. Unfortunately, however, it is impossible to include standard error for mass movement timing due to a lack of metadata.

Volume/mass of mass movements are also an important component of the database, although not of this particular analysis (see Maslin et al., 2004). Relevant data has been taken from articles concerning the event in question. In some cases (notably the Cape Fear slide, Andøya slide, and Canadian Arctic turbidites) assumptions and extrapolations have been made. Specific instances shall be discussed in more detail later, however, whenever assumptions have been made or extrapolation performed this has been justified on a scientific basis.

4. Results

Table 2 is an abbreviated version of the mass movement database; deposits are listed in chronological order. Though included in this table the Canary debris flow and the Madeira abyssal plain 'b' turbidite will not form a part of the further analysis. This is because they may have a volcanic, subareal, trigger (see Masson et al., 1998). As such, they are controlled by different factors than the rest of the events listed.

The latitudinal distribution of these events through time, shown in Fig. 3a, shows a clear trend. Prior to 12 ka calendar years BP most events are mid to low latitude, after 12 ka calendar years BP high-latitude events dominate.

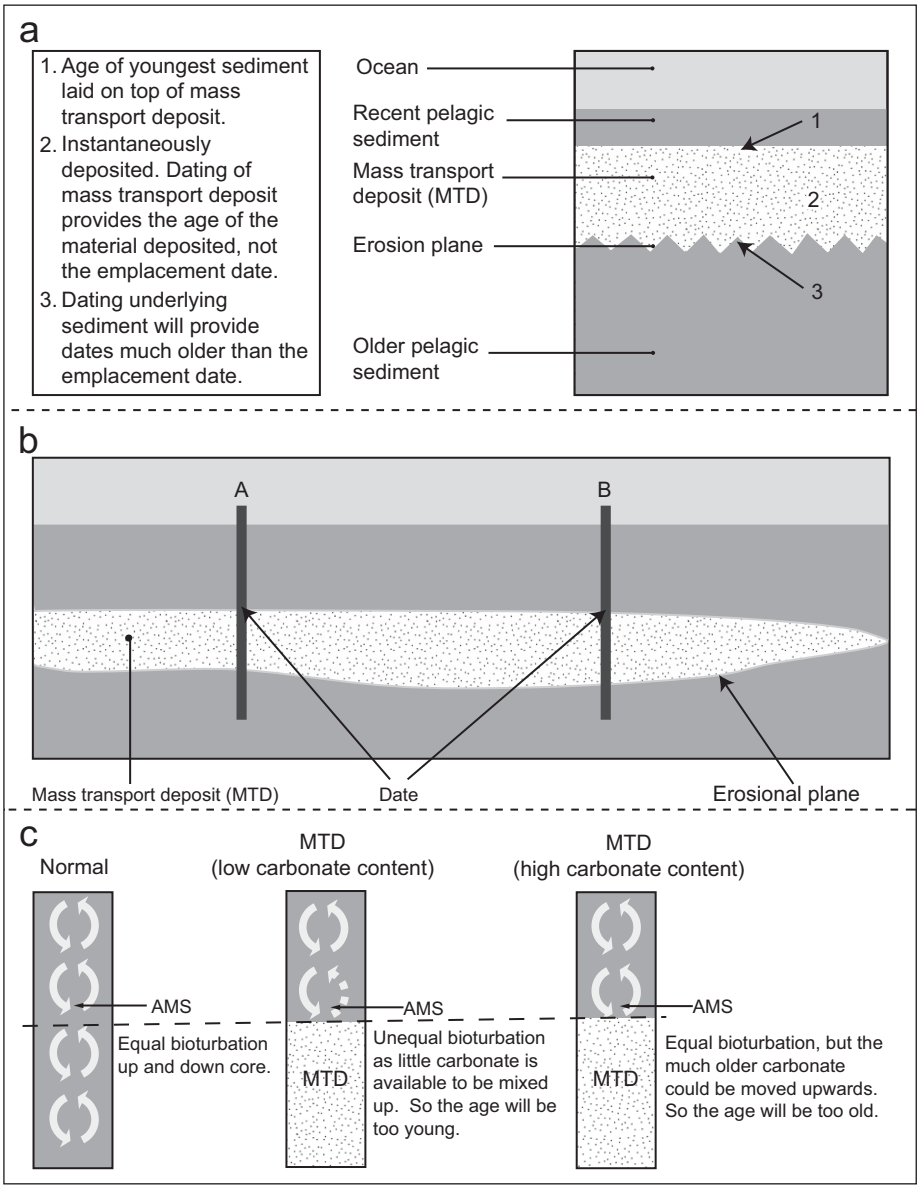

Fig. 2. Dating submarine mass movements: (a) sedimentary column variation, (b) ideal locations of AMS dates and (c) effect of bioturbation.

Fig. 3b shows the occurrence of mass movements in relation to a global mean sea level curve. This graph shows a relatively sparse grouping of events from 45 to 23 ka calendar years BP. From 23 to 14 ka calendar years BP there is a cluster of events associated with the sea level lowstand and Termination 1B. There is a further cluster of events after Termination 1A, followed by a steady grouping of Holocene events.

Fig. 3c shows the relationship between mass movements and Greenland ice core GISP2 CH_4. From 45 to 23 ka calendar years BP mass movements show no clear link with CH_4 peaks. Two events: the Amazon Deep Eastern Mass Transport deposit of the Amazon Fan and the Herodotus Basin Megaturbidite may coincide with CH_4 peaks. However, a further two: the Amazon Deep Western Mass Transport Deposit and the Peach 2 debrite seem to coincide with a CH_4 trough. Following Termination 1B there is a cluster of events associated with the increase of CH_4; however, they are not associated with the preboreal CH_4 peak. Following the Younger Dryas and Termination 1A there is a second cluster of three events (Andøya, Faeroe Slide and Peach 4), which coincide with the early Holocene CH_4 peak. These links between continental slope failure and climate are examined in more detail in the discussion section.

5. Discussion of susceptibility factors and triggering mechanisms affecting the key deposits in the database

These deposits have reasonably well-constrained dates of emplacement, an estimation of volume and they are all large scale ($>25\,km^3$).

Table 2
Late Pleistocene–Holocene submarine mass movements with names, location, type, reliability, volume, original author(s) ascribed cause and reference

Name	Location	Latitude (°N)	Type	Age cal years BP	Reliability	Volume (km^3)	Original author(s) ascribed cause	Reference
Grand Banks turbidite	Sohm abyssal plain	45	Turbidite	70	1	185	Earthquake	Piper and Asku (1987)
Canadian abyssal plain turbidite 1	Canadian abyssal plain	71	Turbidite	1300	4	80	Earthquake	Grantz et al. (1996)
Canadian abyssal plain turbidite 2	Canadian abyssal plain	71	Turbidite	2400	4	80	Earthquake	Grantz et al. (1996)
Canadian abyssal plain turbidite 3a	Canadian abyssal plain	71	Turbidite	3100	4	240	Earthquake	Grantz et al. (1996)
Trænadjupet	North Norwegian continental margin	68	Slide	4000	3	900	Earthquake -post-glacial	Laberg et al. (2000), Laberg et al. (2002)
Canadian abyssal plain turbidite 3b	Canadian abyssal plain	71	Turbidite	6000	4	160	Earthquake	Grantz et al. (1996)
Storegga	West Norwegian continental margin	66	Slide	8100	1	2800	Earthquake -post-glacial, gas hydrates	Jansen et al. (1987), Haflidason et al. (2004).
Canadian abyssal plain turbidite 4	Canadian abyssal plain	71	Turbidite	8200	4	80	Earthquake	Grantz et al. (1996)
Baltimore slide complex	Northeast American margin	38	Slide complex	9400	5	200	Earthquakes, undercutting	Embley (1980, 1982)
Andøya	North Norwegian continental margin	70	Slide	10,000	5	180	Earthquake -post-glacial	Laberg et al. (2000)
Faeroe slide	Northeast Faeroe margin	64	Slide	10,300	4	158	Slope steepening & increased sedimentation	Van Weering et al. (1998)
Peach 4	Barra Fan, Scottish margin	57	Debrite	10,500	4	135	Earthquake	Holmes et al. (1998), Knutz et al. (2001)
BIG '95	Western Mediterranean	40	Debris flow	11,500	4	26	Increased sedimentation & earthquake	Lastras et al. (2002)
Western Debris Flow	Amazon fan	4	Debris flow	13,000	2	2000	Increased sedimentation & changing sea-level	Maslin et al. (1998, 2005), Piper et al. (1997)
Eastern Debris Flow	Amazon fan	4	Debris flow	14,500	2	1500	Increased sedimentation & changing sea-level	Maslin et al. (1998, 2005), Piper et al. (1997)
Madeira abyssal plain 'b' turbidite	Madeira abyssal plain	31	Turbidite	15,000	2	125	Volcanic	Weaver and Rothwell (1987), Weaver et al. (1995
Canary debris flow	Canary island margin	28	Debris flow	15,000	2	400	Volcanic	Masson et al. (1998)
Cape Fear slide	Blake ridge	33	Slide	16,800	3	1700	Gas hydrate, salt daipir intrusion & earthquakes	Popenoe et al. (1991), Paull et al. (1996)
H13 turbidite	Horseshoe abyssal plain	36	Turbidite	17,700	4	33	Earthquake & sea-level change	Lebreiro et al. (1997)
Black shell turbidite	Hatteras abyssal plain	31	Turbidite	18,300	4	100	Increased sedimentation & earthquake	Elmore et al. (1979)
Peach 3	Barra Fan, Scottish margin	57	Debrite	21,000	4	199	Earthquake	Holmes et al. (1998), Knutz et al. (2001)
Balearic abyssal plain megaturbidite	Western Mediterranean	40	Turbidite	22,000	1	500	Earthquake, clathrate release & inc. sedimentation	Rothwell et al. (1998)
Herodotus basin megaturbidite	Southeast Mediterranean	33	Turbidite	27,125	2	400	Tectonic steepening, lowered sea-level & seismic trigger	Reeder et al. (2000)
Deep Eastern MTD	Amazon fan	4	Debris flow	35,000	2	610	Gas hydrate destabilisation	Maslin et al. (1998), Piper et al. (1997)
Peach 2	Barra Fan, Scottish margin	57	Debrite	36,500	4	673	Earthquake	Holmes et al. (1998), Knutz et al. (2001)
Deep Western MTD	Amazon fan	4	Debris flow	43,500	2	630	Gas hydrate destabilisation	Maslin et al. (1998), Piper et al. (1997)

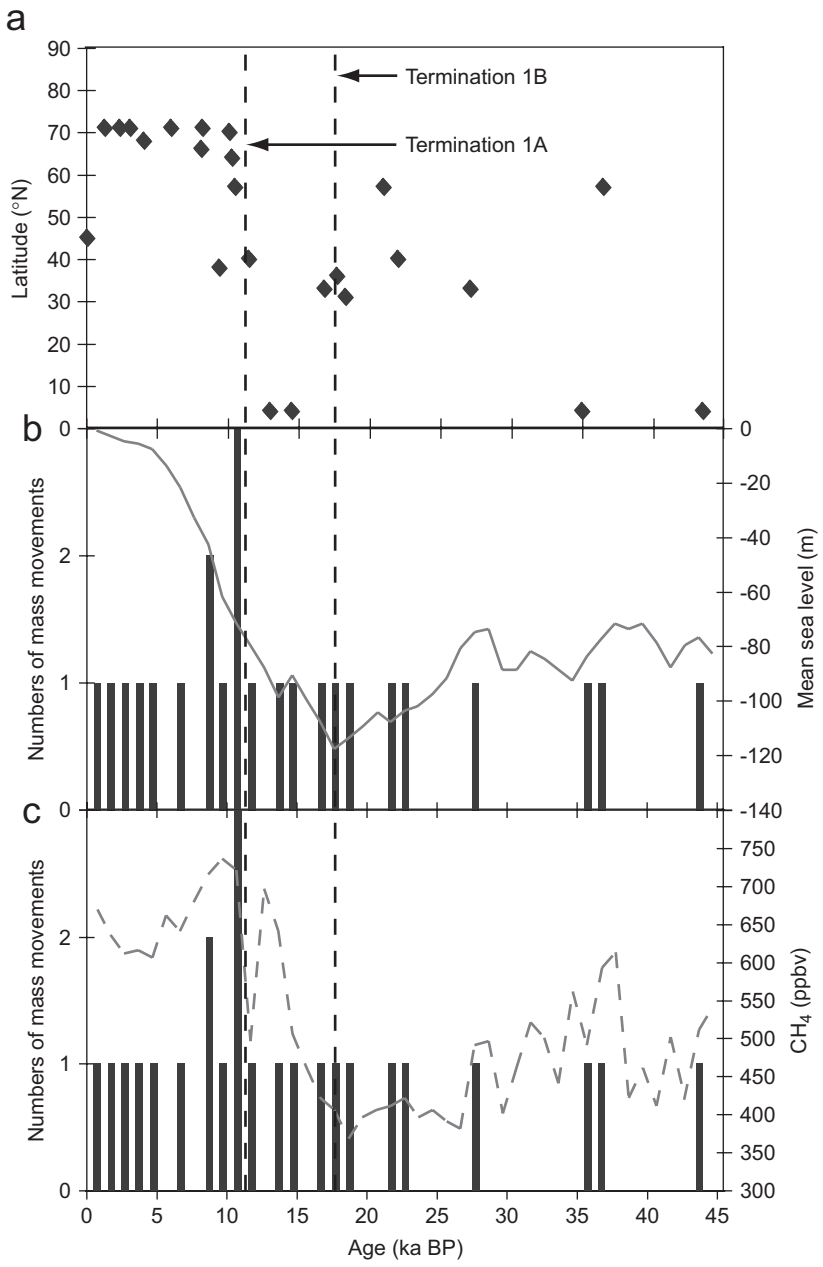

Fig. 3. Latitudinal distribution (a) and timing of submarine mass movements compared with mean global sea level (b) and GISP2 CH_4 (c).

5.1. Northwest european margin

5.1.1. Andøya

In the northeastern Norwegian-Greenland Sea on the Norwegian continental margin proximal to the Lofoten Basin Andøya is a translational slide (Laberg et al., 2000). The slide deposits cover 9700 km^2 and the scar area is approximately 3600 km^2 (Laberg et al., 2000). No precise volume estimates of this slide have been found. However, taking a conservative estimate of 50 m for the headwall scarp (inferred from Laberg et al., 2000, p. 263) a figure of 180 km^3 is obtained (scar area (3600 km^2) × headwall height (0.05 km)). Precise timing of the Andøya slide is not known. 3.5 kHz profiles indicate that there is little or no overlying sediment and the bathymetry reveals a very uneven seafloor (Laberg et al., 2000). This implies that the event is recent. At 4 m depth, in a sediment core from the nearby Andøya Canyon, *Neogloboquadrina pachyderma* offer a AMS ^{14}C date of 8940 ± 150 (corresponding to a calendar date of 10 ka BP), after which pelagic sedimentation dominates (Laberg et al., 2000). This has been taken to represent the age of the event, as shock from the Andøya slide would have caused mass movement in the canyon. The event occurred in the early Holocene after the major part of the deglaciation, shortly after 10 ka calendar years BP most of the Fennoscandinavian ice had retreated (Svendsen and Mangerud, 1987). Susceptibility to mass movement would have been increased by high

sedimentation rates during the deglaciation and slope steepening due to isostasy. Vorren et al. (1998) note that Andøya is situated on the steepest part of the eastern Norwegian-Greenland sea continental margin (5°–18°). An earthquake, associated with the postglacial uplift of Fennoscandinavia, is cited as the most probable trigger due to the events location in an area of comparatively high seismic risk (Laberg et al., 2000).

5.1.2. *Trænadjupet*

On the continental slope east and northeast of the Vøring plateau in the Norwegian-Greenland Sea Trænadjupet is a large translational slide (Laberg and Vorren, 2000; Laberg et al., 2002). Slide scar area is approximately 5000 km^2 and the deposits have been estimated at 900 km^3, assuming an average thickness of 100 m (Laberg et al., 2002). Timing of the event is based on AMS ^{14}C dates from two cores taken from within the scar. Sampling of *Neogloboquadrina pachyderma* indicates that pelagic sedimentation resumed in the slide scar from 4 ka AMS ^{14}C BP (Laberg et al., 2002). This indicates that the event occurred immediately prior to this time postdeglaciation during the mid-Holocene (corresponding to a calendar date of 4 ka BP). from the presence of large blocks and rafts of sediment Laberg and Vorren (2000) argue that failure occurred along surfaces of weakness: most likely interglacial, contouritic, muds possessing relatively high water content and low undrained shear strength. High clay and organic content could lead to excess pore pressure and methane (Laberg and Vorren, 2000). Through geotechnical tests Sultan et al. (2004) established that the contouritic sediments, in which the main failure occurred (Laberg et al., 2003), were particularly weak in undrained conditions appropriate to cohesive failure. Sediment stability would be reduced along these bedding planes and potential for failure increased. Trænadjupet is situated in an area of rapid postglacial fennoscandinavian uplift and high intraplate seismicity (Laberg and Vorren. 2000; Laberg et al., 2000; Fjeldskaar et al., 2000). Martinussen (1961) andøya sea level curve (see Fig. 4a and Fig. 5) demonstrates that rebound is occurring at this time. An earthquake, or succession of small earthquakes, is cited by Laberg and Vorren (2000) as the most likely trigger mechanism. Deglacial sedimentation and isostatic slope steepening would have made the slope more susceptible to failure; an earthquake would have increased the sediment shear stress causing it to fail along the planes of weakness.

5.1.3. *Storegga*

On the Norwegian continental margin south of the Vøring plateau Storegga is a retrogressive, translational slide (Jansen et al., 1987; Bugge et al., 1988; Evans et al., 1996; Haflidason et al., 2004, 2005; Bryn et al., 2005). The slide scar area is 50,000 km^2 and the slide volume has been estimated as between 2400 and 3200 km^3 (Haflidason et al., 2004). It was initially thought that the slide consisted of three separate events: Storegga I (50–30 ka), Storegga II (8–5 ka) and Storegga III (5 ka) (see Jansen et al., 1987; Bugge et al., 1988; Evans et al., 1996). However, it is now believed that all three events occurred simultaneously at 8.1 ka BP (Haflidason et al., 2004; Haflidason et al., 2005). Tsunami deposits have been observed in lake, bog and peat sediments in Norway, Faeroe, Shetland and mainland

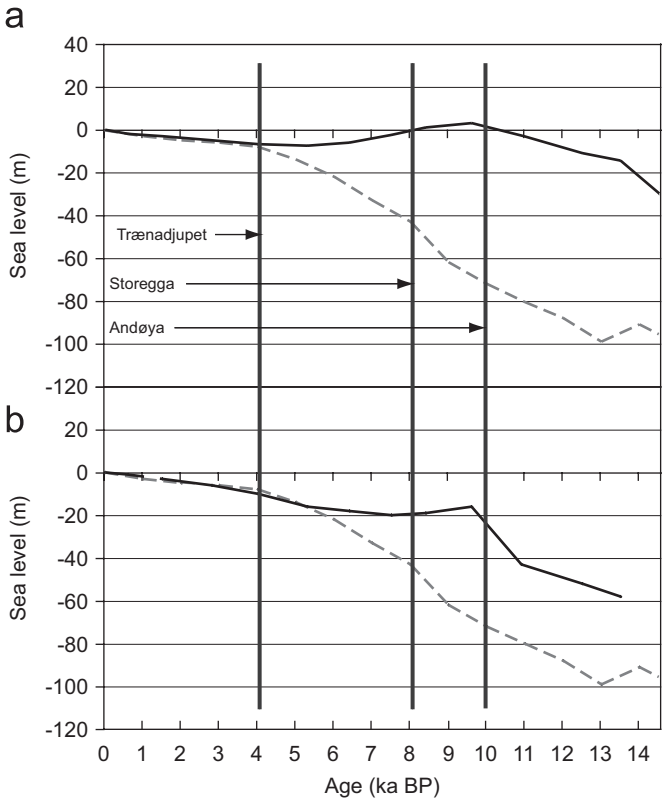

Fig. 4. Comparison of local sea level curves (solid) with mean global sea level (dashed). Norwegian event timing also shown. a. Martinussen's (1961) Andøya curve (~72°N). b. Svendsen and Mangerud's (1987) Frøya curve (~66°N. Global mean sea level from McGuire et al. (1997).

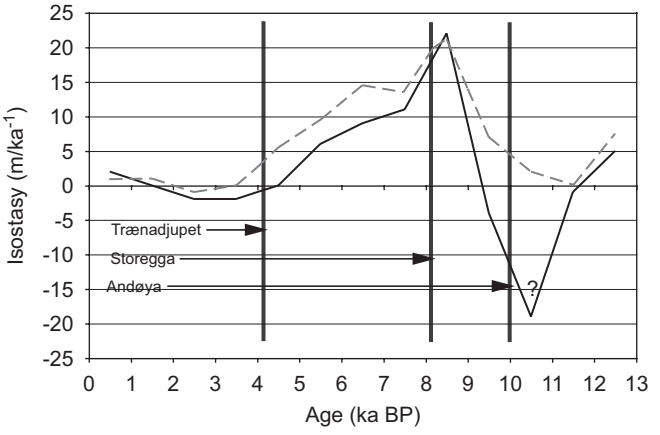

Fig. 5. Approximation of isostatic change of sea level at Frøya (solid) and Andøya (dashed) for the past 12.5 ka. West Norwegian margin mass movements also shown. Isostatic change derived from Martinussen (1961), Svendsen and Mangerud (1987) and McGuire et al. (1997). Value shown is the amount of change for the preceding ka.

Scotland (Bondevik et al., 1997, 2005; Smith et al., 2004). AMS ^{14}C dating of these deposits provides consistent figures of between 7.0 and 7.3 ka AMS ^{14}C BP (Bondevik et al., 2005). Additionally Haflidason et al. (2004) date the slide scar at 7250±250 AMS ^{14}C BP. This corresponds to a calendar age of 8.1 ka BP.

Initial discussion of triggers focused on the role of earthquakes, with a possible facilitating role from gas hydrates (see Bugge et al., 1988; Evans et al., 1996). With the discovery and subsequent development of the Ormen Lange gas field this area has been subject to intense research during recent years. The role of gas hydrates is viewed, at most, as a secondary process: no sign of clathrates have been found in the area's boreholes though some BSRS have been identified (Kvalstad et al., 2005; Mienert et al., 2005). A greater emphasis is placed on the role of glacial sediment loading of the North Sea fan and pore water migration to, and sediment swelling of contouritic marine clays in the distal regions of the storegga slide (see Bryn et al., 2005; Kvalstad et al., 2005). An earthquake is widely regarded as the most likely initial trigger. Research on onshore postglacial faults indicates a magnitude 7 earthquake approximately every 1.1 ka (Bungum et al., 2005). This is postdeglaciation during a period of massive rebound (see Fig. 5) and it is likely that rapid sedimentation and isostatic slope steepening would have increased susceptibility to failure. This region could also be subject to enhanced seismicity from a deglacial seismic pulse migrating from the former forebulge of the Fennoscandian ice-sheet (see Fjeldskaar et al., 2000).

5.1.4. Faeroe slide

Large-scale sliding has occurred on the northeast Faeroe margin, south of the Norwegian basin (Van Weering et al., 1998). No precise volume estimates have been found for this slide. For the purpose of this paper a rough calculation of 158 km^3 has been made (0.2625 km [slump scar height] × (60 km [slump scar width] × 10 km [slump run-out])) from the dimensions described by Van Weering et al. (1998). A single AMS ^{14}C date, 9850±140, was obtained at the foot of the main slump scar on top of compacted and deformed sediments (Van Weering et al., 1998). Multiple sliding events are proposed by Van Weering et al. (1998). The most recent sliding event's early Holocene date, coupled with Van Weering et al. (1998) proposed cause, suggests that the events may have occurred within a relatively short time span. For the purpose of this paper (precise volumes not being the most important factor) the entire 158 km^3 of displaced sediment shall be ascribed the 9850±140 AMS ^{14}C BP (corresponding to a calendar date of 10.3 ka BP), postdeglaciation, date. Van Weering et al. (1998) focus on a combination of subsidence of the Norwegian basin—leading to slope steepening, increased glaciogenic sedimentation from the Faeroese margin and increased sediment supply from contourite currents following the resumption of deep water circulation. These are factors that would have dramatically increased the slope's susceptibility to fail.

5.1.5. Peach slide (debrites 4, 3 and 2)

The Peach slide situated in the Barra Fan, west of Northern Britain, consists of four major debrite units: debrite 4 (135 km^3), debrite 3 (199 km^3), debrite 2 (673 km^3) and debrite 1 (823 km^3) (Holmes et al., 1998). Debrite age has been determined by using the age/depth profile of the Barra Fan constructed by Knutz et al. (2001). Debrite 2 occurred at 36.5 ka calendar years BP, debrite 3 occurred at 21 ka calendar years BP and debrite 4 occurred at 10.5 ka calendar years BP (Maslin et al., 2004). Debrite 2 occurred during the build-up of the British ice sheet, when there was intermittent IRD prior to 30 ka in the Barra Fan (Knutz et al., 2001). Knutz et al. (2001) state that between 21 and 12 ka there were high rates of fine clastic sedimentation and that the glacial ice extended to the outer shelf until 16–17 ka. Debrite 3 occurred just prior to the LGM during high sedimentation that would have increased the slope's susceptibility to failure. Debrite 4 occurred after the deglaciation a period when isostatic seismicity would have been high. Holmes et al. (1998) cite earthquakes as the most likely trigger of the mass movement.

5.2. Mediterranean events

5.2.1. Balearic abyssal plain megaturbidite

The Balearic abyssal plain is situated between the Balearic Islands and Sardinia in the western Mediterranean Sea, it has an area of approximately 60,000 km^2. Rothwell et al. (1998) published evidence of a 500 km^3 megaturbidite covering the abyssal plain. AMS ^{14}C dating of foraminifera and pteropods above and below the deposit yielded a mean age of 18,840 AMS ^{14}C BP; this corresponds to a calendar age of 22 ka BP (Rothwell et al., 1998) correlating with Heinrich event 4 (see Maslin et al., 2004), and a time of lowered sea level prior to the LGM. Rothwell et al. (1998) propose that the trigger for the event may have been related to 'calthrate release and/or earthquake activity, after a long period of accumulation with an increased rate of sediment supply', a factor which would have increased the slope's susceptibility to failure.

5.2.2. BIG'95

The BIG'95 slide deposit is situated on the Ebro margin, on the western side of the Valencia trough: the volume is at least 26 km^3 (Lastras et al., 2002). AMS ^{14}C dating of Foraminifera tests in a hemipelagic unit overlying the slide deposit gives a minimum calendar age of 11.5 ka BP (Lastras et al., 2002) corresponding to the Younger Dryas cooling episode (see Maslin et al., 2004). Four factors are thought to have contributed to the event. Different mechanic behaviour between the underlying volcanic rock and the soft sedimentary cover increased the slope's susceptibility (coupled with sedimentation associated with the deglaciation) to failure. Seismicity, rapid sedimentation

(from the palaeo-Ebro river) leading to overloading and oversteepening of the shelf and enhanced fluid release at the start of the Holocene, due to increased near-bottom water temperature, are potential triggers for the event (Lastras et al., 2002).

5.2.3. Herodotus Basin megaturbidite

The Herodotus basin is situated in the southeastern Mediterranean and has an area of approximately 40,000 km^2. Reeder et al. (2000) documented a megaturbidite with a volume of 400 km^3 in the basin. AMS ^{14}C dating of the overlying pelagic sediment has been used to obtain an emplacement date of 27.1 ka calendar years BP (Reeder et al., 2000) corresponding to Heinrich event 3 (see Maslin et al., 2004). Reeder et al. (2000) propose that a number of factors worked together to trigger the event. A presence of a weak horizon within the sediment column, acting as a glide plane, lowered sea level and tectonic slope steepening increased the slope's susceptibility to failure. Hence Reeder et al. (2000) proposed a seismic trigger.

5.3. Southern European and Northwest African margin

5.3.1. Horseshoe abyssal plain, H_{13} turbidite

The Horseshoe abyssal plain is situated southwest of the Iberian margin. 21,157 km^2 it has a well-preserved record of turbidites, the largest of which (H_{13}) has a volume greater than 33 km^3 (Lebreiro et al., 1997). The provenance of the turbidite was the Portuguese continental shelf (Lebreiro et al., 1997). Lebreiro et al. (1997) demonstrate that the turbidite is situated between Heinrich layers 1 and 2 (14.3 and 21 ka calendar years BP, respectively). Lack of data prevents accurate sedimentation rate assumptions; therefore, a crude emplacement date estimate of 17.7 ka calendar years BP is calculated by taking the mid-chronological point between these layers. Depending on exactly when the event occurred, this is a period just after the LGM with lowered sea levels (possibly rising) and increased sedimentation that would have increased failure susceptibility. Lebreiro et al. (1997) consider the role of earthquakes and sea level change in turbidite emplacement, although they make no attempt to propose a precise trigger.

5.3.2. Madeira abyssal plain 'b' turbidite

The Madeira abyssal plain is situated mid-way between the northwest African margin and the mid-Atlantic ridge and has an area of 68,000 km^2 (Weaver and Rothwell, 1987). The 'b' turbidite has a volume of approximately 125 km^3 (Weaver et al., 1995). Weaver et al. (1995) present evidence revealing that the Canary debris flow is deposited within the basal layer of the turbidite, indicating that the turbidite occurred at the same time as the Canary debris flow. Masson et al. (1998) propose that the Canary debris flow occurred simultaneously with the El Golfo debris avalanche. The date of this debris avalanche has been given as 15 ka calendar years BP (Masson, 1996). Weaver and Rothwell (1987) argue that the turbidite was formed at the distal end of the Canary debris flow and as such the trigger of this event caused the 'b' turbidite. Masson et al. (1998) present evidence demonstrating that the Canary debris flow was probably caused by the collapse of the island flank of Hierro and the resultant sediment loading from the El Golfo debris avalanche. If the arguments of Weaver and Rothwell (1987), and Masson et al. (1998) are correct, the 'b' turbidite was caused by the collapse of the flank of the volcanic island Hierro.

5.3.3. Canary debris flow

The Canary debris flow is situated on the western slopes of the islands La Palma and Hierro, off northwest Africa (Masson et al., 1998). Covering 40,000 km^2 the flow's volume has been estimated at 400 km^3 (Masson et al., 1998). Masson et al. (1998) propose that the debris flow and El Golfo debris avalanche were simultaneous. Masson (1996) provides a date of 15 ka calendar years BP for the debris avalanche; this date can also be ascribed to the debris flow. Masson et al. (1998) argue that either loading of the slope sediments by the debris avalanche or ground accelerations (a consequence of an earthquake associated with the collapse of Hierro) led to sediment failure. In either case the cause of the Canary debris flow can be ascribed to the collapse of the Hierro island flank and the consequent El Golfo debris avalanche's impact on the downslope sediments.

As both the Madeira abyssal plain 'b' turbidite and the Canary Debris Flow are believed to have a volcanic, subareal, origin they shall be omitted from the analysis and discussion, which is primarily concerned with controls acting on the submarine slope.

5.4. Canadian arctic

5.4.1. Canadian abyssal plain turbidites 1, 2, 3a, 3b and 4

Grantz et al. (1996) show a turbidite sequence in the Canadian abyssal plain (Arctic ocean), these turbidites originated on, or from the front of, the Mackenzie delta. Volume has been estimated by multiplying the thickness of the turbidite units by the area of the abyssal plain (200 km × 400 km = 80,000 km^2). This is believed to be valid due to the distal positioning of the core from the turbidite source area. Volume estimates for turbidites 1, 2, 3a, 3b and 4 are 80, 80, 240, 160 and 80 km^3, respectively. Grantz et al. (1996) present an age profile of the turbidite sequence based on AMS ^{14}C dating of *Neogloboquadrina pachyderma*. It is limited by low sedimentation rates and some bioturbation; however, this profile can be used to date the turbidites with relative accuracy. Emplacement dates for turbidites 1, 2, 3a, 3b and 4 as interpreted from the age profile in Grantz et al. (1996) are 1.3, 2.4, 3.1, 6.0 and 8.2 ka calendar years BP respectively. Earthquakes are cited as the most likely trigger of the turbidites, a statement supported by a zone of active seismicity existing beneath the Mackenzie delta and the upper Mackenzie cone (Grantz et al., 1996). During the Holocene (particularly

during the early Holocene) the Mackenzie delta would have been subjected to isostatic forces influencing slope steepness and seisimicity. The deglaciation would have deposited large amounts of sediment increasing the likelihood of overburdening and susceptibility to failure.

5.5. Northeast American margin

5.5.1. Grand Banks turbidite

The Grand Banks turbidite is situated in the Sohm abyssal plain off the northeastern American continental margin. The Laurentian Fan, on the upper continental slope, off St. Pierre Bank, has been identified as the source area (Piper and Asku, 1987; Piper et al., 1999). Piper and Asku (1987) estimated the total volume of the event as 184 km^3. The event broke transatlantic communications cables; this gives us an accurate date of 18th of November 1929 AD, and ties it to a tsunami on the same date (Piper and Asku, 1987; Piper et al., 1999). The trigger mechanism for the event was a magnitude 7.2 earthquake, which led to widespread slumping of the top 20–25 m of sediment and generated the turbidity current (Piper et al., 1999). Piper and Asku (1987) identified coarse-grained sediment, deposited during the deglaciation, in the turbidite deposit. Increased terrestrial sedimentation through the Lawrence River during the Holocene may also have increased the continental slope's susceptibility to failure.

5.5.2. Baltimore canyon slide complex

This slide complex is just south of Baltimore canyon on the eastern United States' continental margin (Embley, 1980). It covers an area of 4000 km^2 and affects the top 50–100 m of sediment (Embley, 1980; Embley, 1982). Assuming a depth of 50 m volume can be estimated, crudely, as 200 km^3. Two sediment cores with AMS ^{14}C dates have been acquired from the head of the slide complex. Two dates of 10,080 and 7285 AMS ^{14}C BP were obtained from clays above the deformed sediment (Embley, 1980). A sample of the slide deposit matrix at the top of the flow yields a AMS ^{14}C date of 11,820 $\pm$ 340 BP (Embley, 1980), indicating that mass movement occurred after this time. The slide complex may have developed over a substantial period of time in a series of discreet events. For the purpose of this paper the mean age of the overlying sediment, 8683 AMS ^{14}C BP (corresponding to a calendar date of 9.4 ka BP), will be taken to represent the age of the slide complex, a date which is postdeglaciation. Trigger mechanisms are discussed by Embley (1982), roles played by earthquakes, gas hydrates and undercutting are all proposed. Occurring after the deglaciation rapid sedimentation would have increased the slope's failure susceptibility through potential overburdening and increased pore pressure.

5.5.3. Black Shell turbidite

The Black Shell turbidite is situated in the Hatteras abyssal plain, off the southeastern United States' continental margin (Elmore et al., 1979). The volume is at least 100 km^3 (Elmore et al., 1979). Coarse shell material within the deposit has been dated using AMS ^{14}C. The youngest age from this sample was 15,855 $\pm$ 260 AMS ^{14}C BP (Elmore et al., 1979). This is the maximum age of the event and for the purpose of this paper this date will be taken to represent the age of the event, placing it just after the LGM. Elmore et al. (1979) suggest that the coalesced deltas of the Susquehanna, Potomac and Neuse rivers failed, initiating a turbidity current. Deglaciation would have increased sedimentation on the deltas and increased failure susceptibility. Elmore et al. (1979) discuss slope oversteepening, which is the factor increasing the susceptibility of the slope to failure, with either a tectonic event or a spring flood acting as the final trigger.

5.5.4. Cape fear slide

The Cape Fear landslide is situated on the continental margin of the southeastern United States, off Cape Fear, North Carolina (Popenoe et al., 1991). The headwall scarp is over 50 km long and 120 m high, the deposits extend 400 km downslope (Popenoe et al., 1991). Popenoe et al. (1991) give dimensions for the upper 70 km of the slide; an approximate volume of 300 km^3 can be calculated for this portion. Extrapolated for the entire 400 km length this yields a volume of 1700 km^3. Samples taken from above an unconformity at 0.5–2.0 m depth within the slide scar yielded ages from 9.0 to 14.5 AMS ^{14}C ka (Paull et al., 1996). If one assumes that pelagic sedimentation resumed just after the event, and that the unconformity represents the top of the slide deposit, then the oldest AMS ^{14}C date is the same age as the Cape Fear slide. Corresponding to a calendar date of 16.8 ka BP, placing the event just after the LGM. A number of likely contributing factors are discussed by Popenoe et al. (1991) including: decomposition of gas hydrate, salt diapir intrusion and earthquakes. The slide deposit is in an area rich in gas hydrates, the combination of the salt diapirs acting as free gas traps and the event occurring during a period of lower sea levels may have weakened the sediments sufficiently for an earthquake to trigger the slide. Increased sedimentation associated with the deglaciation of the North American continent would also have increased the susceptibility to failure.

5.6. Amazon fan

These events are situated in the Amazon fan, Northeast of the Brazilian continental margin (Maslin et al., 1998).

5.6.1. Eastern and Western debris flows

The Western Debris Flow volume has been calculated as 2000 km^3 and the Eastern Debris flow volume has been estimated as approximately 1500 km^3 (Piper et al., 1997). Each event covers an area greater than 15,000 km^2 (Piper et al., 1997; Maslin et al., 1998). These events are capped by Holocene sediments that, according to AMS ^{14}C dating, were deposited between 12 and 14 ^{14}C ka BP (Maslin et al.,

1998). There are potential problems with hiatuses in the sedimentary record (Piper et al., 1997). However, taking the argument of Maslin and Mikkelsen (1997), that there is no interglacial sediment in the underlying top 25 m, they were last active in the early Holocene. Recent information has lead to dates of 13 and 14.5 ka calendar years BP being ascribed to the Western and Eastern Debris Flows respectively (Maslin et al., 2005). It is argued that increased Amazon river sediment discharge, due to the initial deglaciation of the Andes, coupled with the change in sediment deposition centres due to rising sea level loaded the slope and led to oversteepening (Maslin et al., 1998, 2005). These two factors would have increased the susceptibility of the slope to failure.

5.6.2. *Deep Eastern and Deep Western mass transport deposits*

Assuming the thickness of the Deep Eastern deposit is the same as the Deep Western the volume can be calculated as 385 km^3 (7000 $km^2 \times 0.055$ km—figures from Piper et al., 1997). The Lake Mungo palaeomagnetic event is situated above the mass transport deposit, indicating that it is older than 32 ka calendar years BP, and the foraminifera *P. obliquiloculata* is absent, showing that it is younger than 40 ka calendar years BP (Maslin and Mikkelsen, 1997). Maslin et al. (1998) refine the age of the event to 35 ka calendar years BP.

This age corresponds to Heinrich event 4 and falling sea level. The volume of the Deep Western deposit has been calculated as 610 km^3 (Piper et al., 1997). The event occurred between 42 and 45 ka calendar years BP (Maslin et al., 1998). The deposit rests directly on top of interglacial muds, from using sedimentation rate assumptions the age of the top of the deposit is given as approximately 45 ka calendar years BP (Maslin et al., 1998). For this paper an age of 43.5 ka calendar years BP is used for the event, which corresponds to Heinrich event 5 and falling sea level. Destabilisation of gas hydrates and dissociation of calthrates are proposed as the trigger mechanism by Maslin et al. (1998). Supporting evidence exists in the form of the presence of bottom simulating reflectors, indicating the presence of gas hydrates, the origin of the deposited sediment at depths between 200 and 600 below sea level and the timing corresponding to a period when sea levels were falling at a rate of 15–25 m ka^{-1} (Maslin et al., 1998).

6. Discussion of timing of mass movements relative to changes in sea level and climate

The sea level curve shown in Fig. 3B is derived from Barbados and Pacific data (see McGuire et al., 1997). It is more appropriate to use this curve with reference to lower latitude events. This is because high-latitude regions may have been glaciated and as such the relative sea level in these areas are a function of both isostatic and eustatic factors. The Fennoscandian mass movement events are compared with local relative sea level to demonstrate this.

Figs. 4A and B show local relative sea level curves for the last 14.5 ka at Andøya and Frøya, on the west coast of Norway. Fig. 5 shows the approximated rate of Isostatic movement (rebound or depression), calculated by subtracting the rate of global sea level change (from McGuire et al., 1997) from the rate of local sea level change (from Svendsen and Mangerud, 1987; Martinussen, 1961), at these locations.

At Andøya (see Martinussen, 1961) there is a rise in sea level until ~10 ka calendar years BP, between 10 and 5 ka calendar years BP local sea level falls and from 5 ka calendar years BP a slight rise in sea level occurs as the eustatic rise dominates the local sea level. This pattern is explained by the isostatic curve in Fig. 5. At ~11 ka calendar years BP isostatic change appears to be very low, most likely a result of the Younger Dryas re-glaciation. The rate increases to ~7 m ka^{-1} at 10 ka calendar years BP. Isostatic uplift peaks in the period 8–9 ka calendar years BP at ~21 m ka^{-1}, a result of rapid rebound shortly after the final deglaciation. At 7–8 ka calendar years BP there is a reduction in the rate of rebound, though it remains at ~13 m ka^{-1}. Between 6 and 7 ka calendar years BP the rate increases slightly, to ~15 m ka^{-1}, after which the rate decreases steadily until 3 ka calendar years BP when it reaches late Holocene values of ~1 m ka^{-1}.

At Frøya (see Svendsen and Mangerud, 1987) sea level rises steadily until 11 ka calendar years BP, the rate of rise then increases until shortly after 10 ka calendar years BP. There then follows a period of declining sea level until ~7.5 ka calendar years BP, from which point there is a slow rise in sea levels to the present. Fig. 5 shows a decline in the rate of isostatic rise from 12.5 ka calendar years BP. Between 11.5 and 9.5 ka calendar years BP this decline becomes a pronounced negative spike (to −19 m ka^{-1}). It is suspected that this is a false value, resulting in an age offset between the local and global sea level data displayed. From 9.5 ka calendar years BP the figure is more reliable. The peak rate of uplift occurs between 8 and 9 ka calendar years BP at ~22 m ka^{-1}, by 7 ka calendar years BP this has reduced to ~10 m ka^{-1}. From 4 ka calendar years BP rates of uplift are relatively constant at the low Late Holocene levels.

The Andøya slide; At 10 ka calendar years BP; Occurs during the fennoscandian ice-sheet's final stage of retreat (Svendsen and Mangerud, 1987; Bungum et al., 2005). As Fig. 5 demonstrates, this is a period of increasing isostatic uplift. This fact gives backing to laberg et al. (2000) view that the Andøya slide was most likely caused by an isostatic induced earthquake. During periods of ice retreat sedimentation rates tend to be much higher due to melt water discharge, ice-rafting and ice-streams (see Dowdeswell and Elverhøi, 2002). This sedimentation could lead to overburdening and pore fluid migration (Dugan and Flemings, 2000; Biscontin et al., 2004; Strout and Tjelta, 2005). Bungum et al. (2005) argue that a pulse of increased

seisimicity followed immediately from the deglaciation (from 10 ka calendar years BP), most likely with magnitude 7+ earthquakes (richter scale). Situated offshore Norway, on the boundary between the ice sheet and the forebulge region, during the deglaciation and the early Holocene the area would be subject to high rates of crustal stresses and increased seismic activity (Fjeldskaar et al., 2000; Muir-Wood, 2000). It seems likely that, occurring at this time in this location, the Andøya mass movement was caused by the continental slopes being overloaded by sediment during the deglaciation and the triggering of this unstable mass by an isostatic earthquake in a period of, postdeglaciation, heightened seismic activity. Faulting of the continental margin due to continental rebound is also a possible cause (Andøya is situated on the steepest section of the Norwegian-Greenland sea margin with current angles between 5° and 18° (Vorren et al., 1998)). However, a fall in local relative sea level coupled with a rise in sea water temperature of 5 °C (see Birks and Koç, 2002) would have made free gas release from hydrates more probable and it is possible that they played a role.

This isostatic data, combined with the research conducted on the Ormen Lange field, presents an even stronger argument for an earthquake or some form of crustal warping, related faulting, triggering Storrega. The failure occurred at 8.1 ka calendar years BP (see Haflidason et al., 2004, 2005), Fig. 5 demonstrates that this is immediately after the period with the greatest rate of uplift ($>20\,m\,ka^{-1}$), at this time uplift is still $>10\,m\,ka^{-1}$ at Frøya, close to the Storegga slide scar. The event's occurrence would seem to be related to postglacial environmental change: rapid sedimentation (and associated increasing pore pressure) due to the retreat of the Fennoscandinavian ice-sheet, an increase in seismic activity, isostatic-induced slope steepening and potential clathrate destabilisation through warming ocean temperatures.

Trænadjupet occurs, after the local eustatic rise resumes, at 4 ka calendar years BP. Isostatic rebound was still taking place, as noted by Laberg and Vorren (2000) but, as shown in Fig. 5, at a reduced rate. This event is possibly an example of a slope made susceptible to failure during the deglacial environment and then triggered several ka later. It has been argued, based on studies of onshore faults and historical records (see Bungum et al., 2005), that the recurrence time of a Magnitude 7 earthquake on the Norwegian margin is currently approximately 1.1 ka. If such an event occurred in close proximity to the slide area it is quite probable that it would have triggered the event if the slopes were already loaded with unstable sediments. Whilst there is no direct evidence of seismicity occurring offshore Norway during the deglaciation and early Holocene, work by Mörner et al. (2000) documents a suspected Magnitude 8 earthquake in the Iggesund-Hudiksvall area of Sweden, as well as several other magnitude 7 and 8 events occurring in the deglaciation and Holocene, indicating that during this period Fennoscandia was seismically active.

Reinforcing the role of the deglacial environment in facilitating the generation of sedimentary failure, Vanneste et al. (2006) document a large (1350 km^3) mass movement on the northern Svalbard margin: the Hinlopen slide. Timing of the event is not yet known, however, based on geophysical data the authors state that the event is recent, but no later than deglaciation. It seems likely that as more margins are surveyed, and more mass movement events documented, that further evidence for deglacial mass movements will be presented.

When predicting future mass movements on the deglaciating margins of Greenland and Antarctica it is inappropriate to do so with reference to global sea level. Fig. 4 demonstrates very clearly the need to consider local factors such as relative sea level and local sedimentation patterns.

At lower latitude, non-glaciated, margins the McGuire et al. (1997) sea level curve is appropriate. Fig. 6 shows mass movements associated with such margins, mass movements from the northeastern American margin have been omitted because of the influence of the Laurentian ice-sheet. Three events are associated with the deglaciation between 15 and 11.5 ka calendar years BP. Four events occur at regular intervals between 22 and 43.5 ka calendar years BP. The other event occurs either at, or just after, the LGM.

The Amazon Fan events provide a good case study of the low latitude situation (see Piper et al., 1997; Maslin and Mikkelsen, 1997; Maslin et al., 1998, 2005; Maslin and Burns, 2000). The western and eastern debris flows occurred during the deglaciation (Maslin et al., 1998, 2005). Deglaciation of the Andes and increased continental wetness caused a massive increase in Amazon sediment discharge (Maslin et al., 1998; Maslin and Burns, 2000; Maslin et al., 2005). The rising sea level shifted the deposition centre towards the upper continental slope and the Amazon fan, possibly causing overburdening and failure (Maslin et al., 1998, 2005). The deep events occurred earlier during periods of rapidly falling sea level (15–25 m/ka^{-1}). This lower sea level would have increased the susceptibility of the slope to failure. Destabilisation of gas

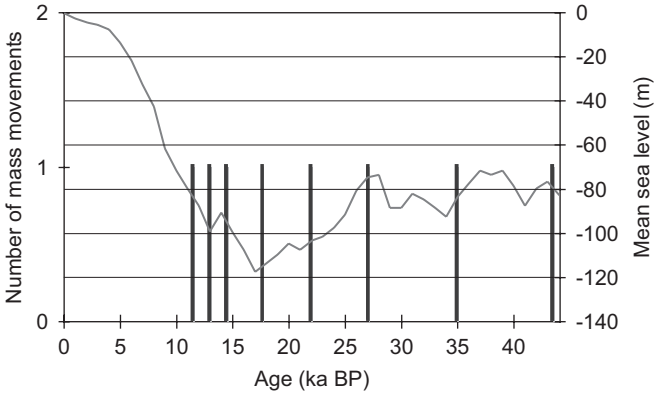

Fig. 6. Low latitude, non-glaciated margin mass movements and mean global sea level curve (from McGuire et al., 1997) for the past 45 ka.

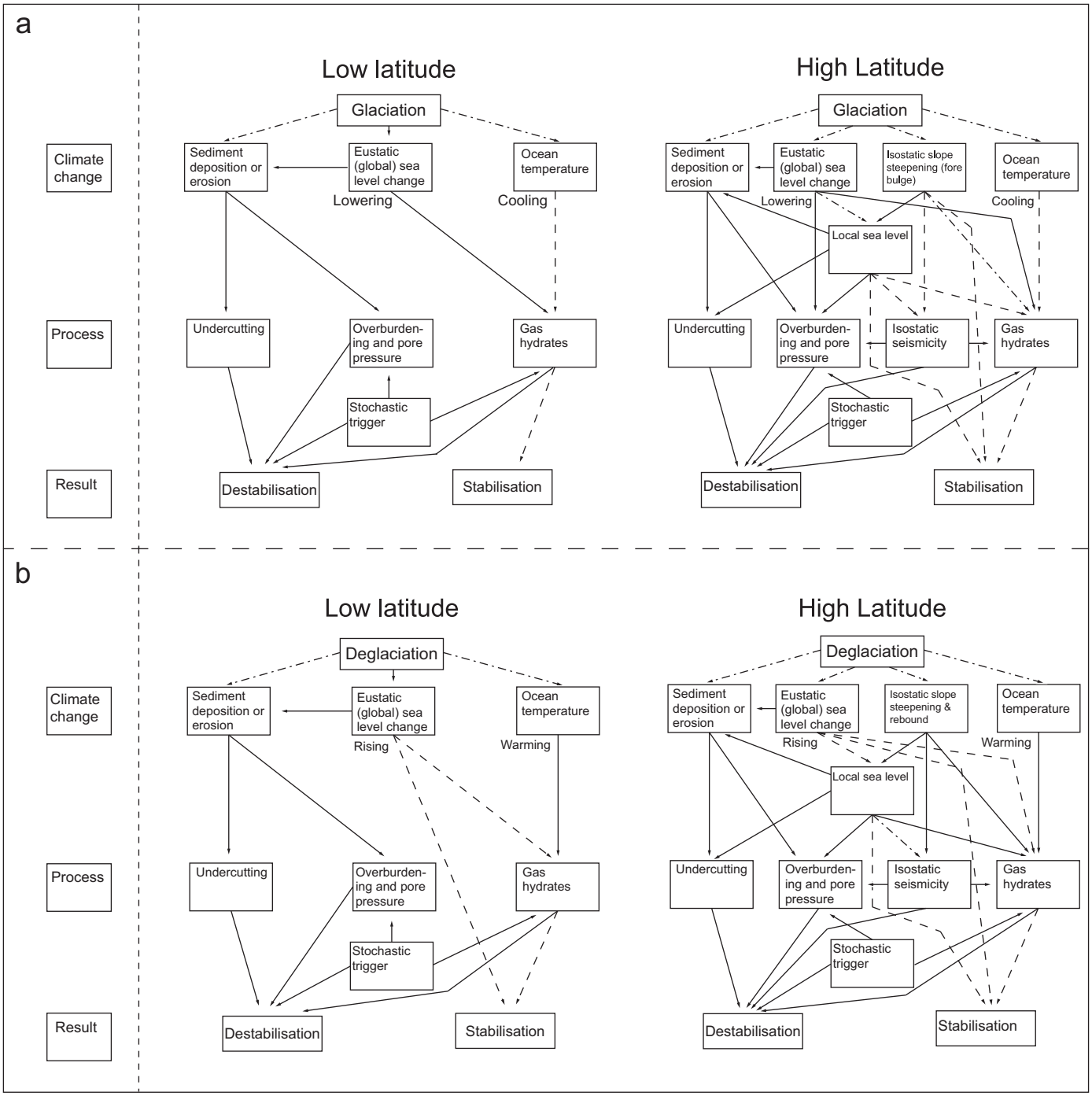

Fig. 7. Flow diagram demonstrating climate change-driven mass movement cause variation. Processes illustrated for both low and high latitudes. Solid lines indicate destabilising, dashed indicate stabilising and dash-dot-dash indicate potentially stabilising or destabilising factors: (a) during glacial periods and (b) during deglacial periods.

hydrates and dissociation of clathrates is the trigger proposed by Maslin et al. (1998, 2005).

6.1. Latitude effects upon susceptibility factors and triggers

Different causal factors operate at different latitudes. These are driven by the flux movement of water between the ocean basins and the continental ice-sheets; and the associated changes in susceptibility and triggering mechanisms that this causes. These different feedbacks are illustrated in Fig. 7.

During the glaciation (Fig. 7a) high-latitude regions experience an increase in ice-mass. This influences sediment deposition (shift from pelagic to glaciogenic), eustatic sea level (falling), isostasy (depression of continental crust due to ice-mass), seisimicity (reduced incidence of earthquakes due to weighting of the continental shelf) and ocean temperatures (cooling). In turn these factors influence the

trigger mechanisms. In this instance gas hydrates are destabilised by the falling eustasy but stabilised by the falling ocean temperature. The combined effects of isostasy and eustasy influence local sea level, which affects gas hydrates, sediment deposition and erosion. Stochastic factors (such as non-isostatic earthquakes) also influence the triggers.

During the deglaciation (Fig. 7b) high-latitude regions experience the collapse of the continental ice-mass. This influences sediment deposition (huge, rapid increase in glaciogenic followed by a return to pelagic (see Dowdeswell and Elverhøi, 2002)), eustatic sea level (rising), isostasy (rebound of depressed continental crust), seismics (pulse of high seisimicity in the forebulge region (Fjeldskaar et al., 2000; Muir-Wood, 2000; Bungum et al., 2005)) and an increase in ocean temperatures (~5 °C in the eastern norwegian sea during the Holocene transition (Birks and Koç, 2002)). The rate of isostatic uplift experienced on some of these margins means that depth of water (and hence pressure) does not increase at the same rate as seawater temperature. This increases the likelihood of destabilised gas hydrates. Rapid sedimentation, release of isostatic forces, an upsurge of seismicity and gas release from hydrates increase stresses operating on the continental margins. High-latitude margins are relatively stable during the glaciation and relatively unstable during deglaciation. In high latitudes during deglaciation local relative sea level will bare little resemblance to mean global relative sea level (see Fig. 4) and, therefore, may have considerable influence on slope stability.

During the glaciation (see Fig. 7a) low-latitude regions experience a fall in ocean temperature and relative sea level, as the ice-mass increases in the high latitudes: influencing sediment deposition (change of deposition centre, see Maslin et al., 1998, 2005). Trigger mechanisms are, therefore, also influenced. Gas hydrates are destabilised by falling sea level but stabilised by cooling temperatures, although temperatures are not reduced to the same degree as in the higher latitudes. A difference in sea surface temperatures of 1.2 °C between the glacial and Holocene is reconstructed by Billups and Spero (1996) for the western equatorial atlantic ocean. the gas hydrate stability zone will be reduced during glacial periods in low latitudes. Change in sediment deposition can lead to overburdening through increasing pore pressures (see Dugan and Flemings, 2000; Biscontin et al., 2004; Strout and Tjelta, 2005).

During the deglaciation (see Fig. 7b) low latitude regions experience a eustatic rise in relative global sea levels due to the melting of the high-latitude ice-mass, sediment deposition will increase due to melting of glaciers in mountains (e.g. Andes and Himalaya) and increased continental wetness (see Maslin et al., 1998; Maslin and Burns, 2000). Gas hydrates will be destabilised by increasing ocean temperatures but stabilised by rising eustatic sea level. Sediment failure is likely to occur due to sediment overburdening resulting from increased rates of sedimentation and shifting deposition centres. Low latitude continental margin slopes will be more susceptible to failures triggered by earthquakes during deglacial periods due to the rapid build up of sediment resulting from the return of interglacial conditions.

7. Conclusions

This paper demonstrates that Late Pleistocene North Atlantic submarine mass movements have been influenced by climatic change through a combination of isostatic and sedimentary processes associated with the oscillating relative sea level. Certain slopes are predisposed to failure because of their sedimentary structure and geological history.

A clear latitudinal zoning exists in the causes of submarine mass movements through the past 45 ka. In the high latitudes during deglaciations, through increased sedimentation, increased ocean temperatures and the release of isostatic energy: increasing the susceptibility of slopes to failure due to isostatic/seismic triggers. In the low latitudes lowered sea relative levels during the glacial increase the probability of failure due to calthrate destabilisation and free gas release (Nisbet, 1990; Haq, 1998; Kennett et al., 2003) and during the deglacial increased sedimentation and changes in deposition centres increase the likelihood of failure due to overburdening of the sedimentary column (see Maslin et al., 1998, 2005). Deglacial submarine mass movements are associated with the early Holocene methane peak.

Climate driven environmental change (with associated changes in local and global relative sea level, sedimentation and isostatic seismicity) is likely to initiate submarine mass movement in the same way as it has in the past. Glacial retreat in Antarctica (see Cook et al., 2005) and Greenland (see Howat et al., 2005; Velicogna and Wahr, 2006) will increase the likelihood of sedimentary failure and mass movements (with their associated impacts of tsunamis and CH_4 release) occurring in these locations.

Acknowledgements

The authors wish to thank: the reviewers Guy Rothwell and another, anonymous, reviewer for their constructive remarks; Dave Long and Richard Holmes for help and advice. Matthew Owen thanks the UCL Graduate School, ECRC R&D fund and ENSIS trust fund for funding the research.

References

Bea, R.G., Wright, S.G., Sircar, P., Niedoroda, A.W., 1983. Wave-induced slides in South Pass Block 70, Mississippi Delta. Journal of Geotechnical Engineering 109 (4), 619–644.

Billups, K., Spero, H.J., 1996. Reconstructing the stable isotope geochemistry and paleotemperatures of the equatorial Atlantic during the last 150,000 years: results from individual foraminifera. Paleoceanography 11 (2), 217–238.

Birks, C.J.A., Koç, N., 2002. A high-resolution diatom record of late-Quaternary sea-surface temperatures and oceanic conditions from the eastern Norwegian Sea. Boreas 31, 323–344.

Biscontin, G., Pestana, J.M., Nadim, F., 2004. Seismic triggering of submarine slides in soft cohesive soil deposits. Marine Geology 203, 341–354.

Bondevik, S., Svendsen, J.I., Johnsen, G., Mangerud, J., Kaland, P.E., 1997. The Storegga tsunami along the Norwegian coast, its age and runup. Boreas 26, 29–53.

Bondevik, S., Løvholt, F., Harbitz, C., Mangerud, J., Dawson, A., Svendsen, J.I., 2005. The Storegga Slide tsunami—comparing field observations with numerical simulations. Marine and Petroleum Geology 22, 195–208.

Boulay, S., Colin, C., Trentesaux, A., Frank, N., Liu, Z., 2005. Sediment sources and East Asian monsoon intensity over the last 450 ky, Mineralogical and geochemical investigations on South China Sea sediments. Palaeogeography, Palaeoclimatology, Palaeoecology, 228, 260–277.

Bryn, P., Berg, K., Stoker, M.S., Haflidason, H., Solheim, A., 2005. Contourites and their relevance for mass wasting along the mid-Norwegian Margin. Marine and Petroleum Geology 22, 85–96.

Bugge, T., Belderson, R.H., Kenyon, N.H., 1988. The Storegga slide. Philosophical Transactions of the Royal Society London A 325, 357–388.

Bungum, H., Lindholm, C., Faleide, J.I., 2005. Postglacial seisimicity offshore mid-Norway with emphasis on spatio-temporal-magnitudal variations. Marine and Petroleum Geology 22, 137–148.

Carey, S., 1997. Influence of convective sedimentation on the formation of widespread tephra fall layers in the deep sea. Geology 25 (9), 839–842.

Coleman, J.M., Walker, H.J., Grabau, W.E., 1998. Sediment instability in the Mississippi River delta. Journal of Coastal Research 14 (3), 872–881.

Cook, A.J., Fox, A.J., Vaughan, D.G., Ferrigno, J.G., 2005. Retreating Glacier fronts on the Antarctic Peninsula over the past half-century. Science 308, 541–544.

Day, S., Maslin, M.A., 2005. Linking large impacts, gas hydrates and carbon isotope excursions through widespread sediment liquifaction and continental slope failure: the example of the K–T boundary: event. In: Kenkmann, T., Horz, F., Deutsch, A. (Eds.), Large Impacts III. Geological Society of America Special Paper, vol. 384, pp. 239–258.

Dickens, G.R., 2003. Rethinking the global carbon cycle with a large, dynamic and microbially mediated gas hydrate capacitor. Earth and Planetary Science Letters 213, 169–183.

Dowdeswell, J.A., Elverhøi, A., 2002. The timing of initiation of fast-flowing ice streams during a glacial cycle inferred from glacimarine sedimentation. Marine Geology 188, 3–14.

Dugan, B., Flemings, P.B., 2000. Overpressure and fluid flow in the New Jersey continental slope: implications for slope failure and cold seeps. Science 289, 288–291.

Elmore, R.D., Pilkey, O.H., Cleary, W.J., Curran, H.A., 1979. Black Shell turbidite, Hatteras Abyssal Plain, western Atlantic Ocean. Geological Society of America Bulletin 90, 1165–1176.

Embley, R.W., 1980. The role of mass transport in the distribution and character of deep-ocean sediments with special reference to the North Atlantic. Marine Geology 38, 23–50.

Embley, R.W., 1982. Anatomy of some Atlantic margin sediment slides and some comments on ages and mechanisms. In: Saxov, S., Nieuwenhuis, J.K. (Eds.), Marine Slides and other Mass Movements. NATO, New York, pp. 189–213.

Evans, D., King, E.L., Kenyon, N.H., Brett, C., Wallis, D., 1996. Evidence for long-term instability in the Storegga Slide region off western Norway. Marine Geology 130, 281–292.

Evans, D., Harrison, Z., Shannon, P.M., Laberg, J.S., Nielsen, T., Ayers, S., Holmes, R., Hoult, R.J., Lindberg, B., Haflidason, H., Long, D., Kuijers, A., Andersen, E.S., Bryn, P., 2005. Palaeoslides and other mass failures of Pliocene to Pleistocene age along the Atlantic continental margin of NW Europe. Marine and Petroleum Geology 22, 1131–1148.

Fjeldskaar, W., Lindholm, C., Dehls, J.F., Fjeldskaar, I., 2000. Postglacial uplift, neotectonics and seismicity in Fennoscandia. Quaternary Science Reviews 19, 1413–1422.

Garagesh, I.A., Lobkovskii, L.I., Kozgrev, D.R., Mazova, R.Kh., 2003. Generation and runup of Tsunami waves at an submarine landslide. Oceanology 43 (2), 173–181.

Gee, M.J.R., Masson, D.G., Watts, A.B., Allen, P.A., 1999. The Saharan debris flow: an insight into the mechanics of a long runout submarine debris flows. Sedimentology 42 (6), 957–974.

Grantz, A., Phillips, R.L., Mullen, M.W., Starratt, S.W., Jones, G.A., Naidu, A.S., Finney, B.P., 1996. Character, paleoenvironment, rate of accumulation, and evidence for seismic triggering of Holocene turbidites, Canada abyssal plain, Arctic Ocean. Marine Geology 133, 51–73.

Haflidason, H., Sejrup, H.P., Nygård, A., Mienert, J., Bryn, P., Lien, R., Forsberg, C.F., Berg, K., Masson, D., 2004. The Storegga slide: architecture, geometry and slide development. Marine Geology 213, 201–234.

Haflidason, H., Lien, R., Sejrup, H.P., Forsberg, C.F., Bryn, P., 2005. The dating and morphometry of the Storegga Slide. Marine and Petroleum Geology 22, 123–136.

Hampton, M.A., Lee, H.J., Locat, J., 1996. Submarine landslides. Reviews of Geophysics 34 (1), 33–59.

Haq, B.U., 1998. Natural gas hydrates: searching the long-term climatic and slope stability records. In: Henriet, J.-P., Meinert, J. (Eds.), Gas Hydrates: Relevance to World Margin Stability and Climate Change. Geological Society, London, Special Publications, vol. 137, pp. 303–318.

Hesse, R., Rashid, H., Khodabakhsh, S., 2004. Fine-grained sediment lofting from meltwater-generated turbidity currents during Heinrich events. Geology 32 (5), 449–452.

Holmes, R., Long, D., Dodd, L.R., 1998. Large-scale debrites and submarine landslides on the Barra Fan, west of Britain. In: Stoker, M.S., Evans, D., Cramp, A. (Eds.), Geological Processes on Continental Margins: Sedimentation, Mass Wasting and Stability. Geological Society, London, Special Publications, vol. 129, pp. 67–79.

Howat, I.M., Joughin, I., Tulaczyk, S., Gogineni, S., 2005. Rapid retreat and acceleration of Helheim Glacier, east Greenland. Geophysical Research Letters 32, L22502.

Jansen, E., Befring, S., Bugge, T., Eidvin, T., Holtedahl, H., Sejrup, H.P., 1987. Large submarine slides on the Norwegian continental margin: sediments, transport and timing. Marine Geology 78, 77–107.

Jeng, D.S., 2001. Mechanism of the wave-induced seabed instability in the vicinity of a breakwater: a review. Ocean Engineering 28, 537–570.

Kennett, J., Cannariato, K.G., Hendy, I.L., Behl, R.J., 2003. Methane hydrates in Quaternary climate Change: The Clathrate Gun Hypothesis. American Geophysical Union, Washington, DC, 216pp.

Knutz, P.C., Austin, W.E.N., Jones, E.J.W., 2001. Millennial-scale depositional cycles related to British Ice Sheet variability and North Atlantic paleocirculation since 45 kyr BP, Barra Fan, UK margin. Paleoceanography 16 (1), 53–64.

Kvalstad, T.J., Andresen, L., Forsberg, C.F., Berg, K., Bryn, P., Wangen, M., 2005. The Storegga slide: evaluation of triggering sources and slide mechanics. Marine and Petroleum Geology 22, 245–256.

Kvenvolden, K.A., 1993. Gas hydrates—geological perspective and global change. Reviews of Geophysics 31 (2), 173–187.

Kvenvolden, K.A., 1998. A primer on the geological occurrence of gas hydrate. In: Henriet, J.-P., Mienert, J. (Eds.), Gas Hydrates: Relevance to World Margin Stability and Climate Change. Geological Society, London, vol. 137, pp. 9–30.

Laberg, J.S., Vorren, T.O., 2000. Trænadjupet slide, offshore Norway—morphology, evacuation and triggering mechanisms. Marine Geology 171, 95–114.

Laberg, J.S., Vorren, T.O., Dowdeswell, J.A., Kenyon, N.H., Taylor, J., 2000. The Andøya slide and the Andøya Canyon, north-eastern Norwegian-Greenland Sea. Marine Geology 162, 259–275.

Laberg, J.S., Vorren, T.O., Mienert, J., Evans, D., Lindberg, B., Ottesen, D., Kenyon, N.H., Henriksen, S., 2002. Late Quaternary palaeoenvironment and chronology in the Trænadjupet slide area offshore Norway. Marine Geology 188, 35–60.

Laberg, J.S., Vorren, T.O., Mienert, J., Haflidason, H., Bryn, P., Lien, R., 2003. Preconditions leading to the Holocene Trænadjupet Slide offshore Norway. In: Locat, J., Mienert, J. (Eds.), Advances in Natural and Technological Hazards Research. Kluwer, Dordrecht, The Netherlands, pp. 247–254.

Lastras, G., Canals, M., Hughes-Clarke, J.E., Moreno, A., De Batist, M., Masson, D.G., Cochonat, P., 2002. Seafloor imagery from the BIG'95 debris flow, western Mediterranean. Geology 30 (10), 871–874.

Lay, T., Kanamori, H., Ammon, C.J., Nettles, M., Ward, S.N., Aster, R.C., Beck, S.L., Bilek, S.L., Brudzinski, M.R., Butler, R., DeShon, H.R., Ekström, G., Satake, K., Sipkin, S., 2005. The Great Sumatra-Andaman Earthquake of 26 December 2004. Science 308, 1127–1133.

Lebreiro, S.M., McCave, I.N., Weaver, P.P.E., 1997. Late Quaternary turbidite emplacement on the Horseshoe abyssal plain (Iberian margin). Journal of Sedimentary Research 67 (5), 856–870.

Little, M.G., Schneider, R.R., Kroon, D., Price, B., Summerhayes, C.P., Segl, M., 1997. Trade wind forcing of upwelling, seasonality, and Heinrich events as a response to sub-Milankovitch climate variability. Paleoceanography 12 (4), 568–576.

Locat, J., 2001. Instabilities along ocean margins: a geomorphological and geotechnical perspective. Marine and Petroleum Geology 18, 503–512.

Locat, J., Lee, H.J., Locat, P., Imran, J., 2004. Numerical analysis of the mobility of the Palos Verdes Debris avalanche, California, and its implications for the generation of tsunamis. Marine Geology 203 (3–4), 269–280.

Loubere, P., Meyers, P., Gary, A., 1995. Benthic foraminiferal microhabitat selection, carbon isotope values, and association with larger animals: a test with *Uvigerina peregrina*. Journal of Foraminiferal Research 25 (1), 1107–1110.

Martel, S.J., 2004. Mechanics of landslide initiation as a shear fracture phenomenon. Marine Geology 203, 319–339.

Martinussen, M., 1961. C14-datings referring to shorelines, transgressions and glacial substages in Northern Norway. Norges Geologiske, Undersökelse 215, 37–67.

Maslin, M., Burns, S.J., 2000. Reconstruction of the Amazon basin effective moisture availability over the last 14000 yr. Science 290, 2285–2287.

Maslin, M., Mikkelsen, N., 1997. Amazon fan mass-transport deposits and underlying interglacial deposits: age estimates and fan dynamics. Proceedings of the Ocean Drilling Program, Scientific Results 155, 353–365.

Maslin, M., Mikkelsen, N., Vilela, C., Haq, B., 1998. Sea-level- and gas-hydrate-controlled catastrophic sediment failures of the Amazon fan. Geology 26 (12), 1107–1110.

Maslin, M., Owen, M., Day, S., Long, D., 2004. Linking continental-slope failures and climate change: testing the clathrate gun hypothesis. Geology 32 (1), 53–56.

Maslin, M., Vilela, C., Mikkelsen, N., Grootes, P., 2005. Causes of catastrophic sediment failures of the Amazon Fan. Quaternary Science Reviews 24, 2180–2193.

Masson, D.G., 1996. Catastrophic collapse of the volcanic island of Hierro 15 ka ago and the history of landslides in the Canary Islands. Geology 24 (3), 231–234.

Masson, D.G., Canals, M., Alonso, B., Urgeles, R., Huhnerbach, V., 1998. The Canary Debris Flow: source area morphology and failure mechanisms. Sedimentology 45, 411–432.

McGuire, W.J., Howarth, R.J., Firth, C.R., Solow, A.R., Pullen, A.D., Saunders, S.J., Stewart, I.S., Vita-Finzi, C., 1997. Correlation between rate of sea-level change and frequency of explosive volcanism in the Mediterranean. Nature 389, 473–476.

Mienert, J., Posewang, J., Baumann, M., 1998. Gas hydrates along the northeastern Atlantic margin: possible hydrate-bound margin instabilities and possible release of methane. In: Henriet, J.-P., Mienert, J. (Eds.), Gas Hydrates: Relevance to World Margin Stability and Climate Change. Geological Society, London, Special Publications, vol. 137, pp. 275–291.

Mienert, J., Vanneste, M., Bünz, S., Andreassen, K., Haflidason, H., Sejrup, H.P., 2005. Ocean warming and gas hydrate stability on the mid-Norwegian margin at the Storegga Slide. Marine and Petroleum Geology 22, 233–244.

Mörner, N.-A., Tröften, P.E., Sjöberg, R., Grant, D., Dawson, S., Bronge, C., Kvamsdal, O., Sidén, A., 2000. Deglacial paleoseismicity in Sweden: the 9663 BP Iggesund event. Quaternary Science Reviews 19, 1461–1468.

Muir-Wood, R., 2000. Deglaciation Seismotectonics: a principle influence on intraplate seismogenesis at high latitudes. Quaternary Science Reviews 19, 1399–1411.

Nisbet, E.G., 1990. The end of the ice age. Canadian Journal of Earth Sciences 27, 148–157.

Norris, R.D., Röhl, U., 1999. Carbon cycling and chronology of climate warming during the Paleocene/Eocene transition. Nature 401, 775–778.

Orange, D.L., Breen, N.A., 1992. The effects of fluid escape on Accretionary Wedges, 2: seepage force, slope failure, headless submarine canyons, and vents. Journal of Geophysical Research 97 (B6), 9277–9295.

Paull, C.K., Ussler III, W., Dillon, W., 1991. Is the extent of glaciation limited by marine gas hydrates. Geophysical Research Letters 18, 432–434.

Paull, C.K., Buelow, W.J., Ussler III, W., Borowski, W.S., 1996. Increased continental-margin slumping frequency during sea-level lowstands above gas hydrate-bearing sediments. Geology 24 (2), 143–146.

Paull, C.K., Brewer, P.G., Ussler III, W., Peltzer, E.T., Redher, G., Clague, D., 2003. An experiment demonstrating that marine slumping is a mechanism to transfer methane from seafloor gas-hydrate deposits into the upper ocean and atmosphere. Geo-Marine Letters 22, 198–203.

Piper, D.J.W., Asku, A.E., 1987. The source and origin of the 1929 Grand Banks turbidity current inferred from sediment budgets. Geo-Marine Letters 7, 177–182.

Piper, D.J.W., Primez, C., Manley, P.L., Long, D., Flood, R.D., Normark, W.R., Showers, W., 1997. Mass-transport deposits of the Amazon fan. Proceedings of the Ocean Drilling Program, Scientific Results 155, 109–146.

Piper, D.J.W., Cochonat, P., Morrison, M.L., 1999. The sequence of events around the epicentre of the 1929 Grand Banks earthquake: initiation of debris flows and turbidity current inferred from sidescan sonar. Sedimentology 46, 79–97.

Popenoe, P., Schmuck, E.A., Dillon, W.P., 1991. The Cape Fear landslide: slope failure associated with salt diapirism and gas hydrate decomposition. USGS Bulletin, No. 2002, pp. 40–53.

Prins, M.A., Postma, G., 2000. Effects of climate, sea level, and tectonics unraveled for last deglaciation turbidite records of the Arabian Sea. Geology 28 (4), 375–378.

Rabinovich, A.B., Thomson, R.E., Kulikov, E.A., Bornhold, B.D., Fine, I.V., 1999. The landslide-generated tsunami of November 3, 1994 in Skagway Harbor, Alaska: a case study. Geophysical Research Letters 26 (19), 3009–3012.

Reeder, M.S., Rothwell, R.G., Stow, D.A.V., 2000. Influence of sea level and basin physiography on emplacement of the late Pleistocene Herodotus Basin Megaturbidite, SE Mediterranean Sea. Marine and Petroleum Geology 17, 199–218.

Rothwell, R.G., Thomson, J., Kähler, G., 1998. Low-sea-level emplacement of a very large Late Pleistocene 'megaturbidite' in the western Mediterranean Sea. Nature 392, 377–380.

Smith, D.E., Shi, S., Cullingford, R.A., Dawson, A.G., Dawson, S., Firth, C.R., Foster, I.D.L., Fretwell, P.T., Haggart, B.A., Holloway, L.K., Long, D., 2004. The Holocene Storegga Slide tsunami in the United Kingdom. Quaternary Science Reviews 23, 2291–2321.

Sparks, R.S.J., Bonnecaze, R.T., Huppert, H.E., Lister, J.R., Hallworth, M.A., Mader, H., Phillips, J., 1993. Sediment-laden gravity currents with reversing buoyancy. Earth and Planetary Science Letters 114 (2–3), 243–257.

Stoker, M.S., Leslie, A.B., Scott, W.D., Briden, J.C., Hine, N.M., Harland, R., Wilkinson, I.P., Evans, D., Ardus, D.A., 1994. A record of late Cenozoic stratigraphy, sedimentation and climate change from

the Hebrides Slope, NE Atlantic Ocean. Journal of the Geological Society 151, 235–249.

Strout, J.M., Tjelta, T.I., 2005. In situ pore pressures: what is their significance and how can they be reliably measured? Marine and Petroleum Geology 22, 275–285.

Stuiver, M., Reimer, P.J., 1993. Extended C-14 data-base and revised calib 3.0 C-14 age calibration program. Radiocarbon 35 (1), 215–230.

Sultan, N., Cochonat, P., Canals, M., Cattaneo, A., Dennielou, B., Haflidason, H., Laberg, J.S., Long, D., Mienert, J., Trincardi, F., Urgeles, R., Vorren, T.O., Wilson, C., 2004. Triggering mechanisms of slope instability processes and sediment failures on continental margins: a geotechnical approach. Marine Geology 213, 291–321.

Svendsen, J.I., Mangerud, J., 1987. Late Weichselian and Holocene sea-level history for a cross section of western Norway. Journal of Quaternary Science 2, 113–132.

Tappin, D.R., Watts, P., McMurty, G.M., Lafoy, Y., Matsumoto, T., 2001. The Sissano, Papua New Guinea tsunami of July 1998—offshore evidence on the source mechanism. Marine Geology 175 (1), 1–23.

Van Weering, T.C.E., Nielsen, T., Kenyon, N.H., Akentieva, K., Kuijupers, A.H., 1998. Large submarine slides on the NE Faeroe continental margin. In: Stoker, M.S., Evans, D., Cramp, A. (Eds.), Geological Processes on Continental Margins: Sedimentation, Mass Wasting and Stability. Geological Society, London, Special Publications, vol. 129, pp. 5–17.

Vanneste, M., Mienert, J., Bünz, S., 2006. The Hinlopen Slide: a giant, submarine slope failure on the northern Svalbard margin, Arctic Ocean. Earth and Planetary Science Letters 245, 373–388.

Velicogna, I., Wahr, J., 2006. Acceleration of Greenland ice mass loss in spring 2004. Nature 443, 329–331.

Volpi, V., Camerlenghi, A., Hillenbrand, C.-D., Rebesco, M., Ivaldi, R., 2003. Effects of biogenic silica on sediment compaction and slope stability on the pacific margin of the Antarctic Peninsula. Basin Research 15, 339–363.

Von Rad, U., Tahir, M., 1997. Late Quaternary sedimentation on the outer Indus shelf and slope (Pakistan): evidence from high-resolution seismic data and coring. Marine Geology 138, 193–236.

Vorren, T.O., Laberg, J.S., Blaume, F., Dowdeswell, J.A., Kenyon, N.H., Mienert, J., Rumohr, J., Werner, F., 1998. The Norwegian-Greenland Sea continental margins: morphology and late Quaternary sedimentary processes and environment. Quaternary Science Reviews 17, 273–302.

Walsh, J.P., Corbett, D.R., Mallinson, D., Goni, M., Dail, M., Loewy, C., Marciniak, K., Ryan, K., Smith, C., Stevens, A., Sumners, B., Tesi, T., 2006. Mississippi Delta Mudflow activity and 2005 Gulf Hurricanes. EOS 87 (44), 477–479.

Weaver, P.P.E., Rothwell, R.G., 1987. Sedimentation on the Madeira abyssal plain over the last 300,000 years. In: Weaver, P.P.E., Thomson, J. (Eds.), Geology and Geochemistry of Abyssal Plains. Geological Society, London, Special Publications, vol. 31, pp. 71–86.

Weaver, P.P.E., Masson, D.G., Gunn, D.E., Kidd, R.B., Rothwell, R.G., Maddison, D.A., 1995. Sediment mass wasting in the Canary Basin. In: Pickering, K.T., Hiscott, R.N., Kenyon, N.H., Ricci Lucchi, F., Smith, R.D.A. (Eds.), Atlas of Deep Water Environments: Architectural Style in Turbidite Systems. Chapman & Hall, London, pp. 287–296.

Weber, M.E., Wiedicke-Hombach, M., Kudrass, H.R., Erlenkeuser, H., 2003. Bengal Fan sediment transport activity and response to climate forcing inferred from sediment physical properties. Sedimentary Geology 155, 361–381.

Wilson, C.K., Long, D., Bulat, J., 2004. The morphology, setting and processes of the Afen Slide. Marine Geology 213, 149–167.

Wright, S.G., Rathje, E.M., 2003. Triggering mechanisms of slope instability and their relationship to Earthquakes and Tsunamis. Pure and Applied Geophysics 160, 1865–1877.

Zachos, J., Pagani, M., Sloan, L., Thomas, E., Billups, K., 2001. Trends, rhythms, and aberrations in global climate 65 Ma to present. Science 292, 686–693.